SHEAR DESIGN AND ASSESSMENT OF REINFORCED AND PRESTRESSED CONCRETE BEAMS BASED ON A MECHANICAL MODEL

Antonio Marí[1], Jesús M. Bairán[2], Antoni Cladera[3], and Eva Oller[4]

Corresponding autor: Antonio Marí. antonio.mari@upc.edu

Abstract

Safe and economical design and assessment of reinforced (RC) and prestressed concrete (PC) beams requires the availability of accurate but simple formulations which adequately capture the structural response. In this paper, a mechanical model for the prediction of the shear-flexural strength of PC and RC members with rectangular, I or T sections, with and without shear reinforcement, is presented. The model is based on the principles of concrete mechanics and on assumptions supported by the observed experimental behavior and by the results of refined numerical models. Compact, simple and accurate expressions are derived for design and verification of the shear strength, which incorporate the most relevant shear transfer actions. Excellent agreement between the predictions of the model and the results of the recently published ACI-DAfStb databases, including more than 1287 tests on RC and PC beams with and without stirrups, has been observed. The theory behind the model provides consistent explanations for many aspects related to the shear response that are not clearly explained by current code formulations, making it a very helpful tool for daily engineering practice.

[1] Professor, Construction Engineering Department, Universitat Politècnica de Catalunya, Jordi Girona 1-3, C-1 201, 08034 Barcelona (Spain), antonio.mari@upc.edu

[2] Associate Professor, Construction Engineering Department, Universitat Politècnica de Catalunya, Jordi Girona 1-3, C-1 201, 08034 Barcelona (Spain), jesus.miguel.bairan@upc.edu

[3] Associate Professor, Physics Department, Universitat de les Illes Balears, Ctra. Valldemossa km 7.5, 07122 Palma de Mallorca (Spain), antoni.cladera@uib.es

[4] Assistant Professor, Construction Engineering Department, Universitat Politècnica de Catalunya, Jordi Girona 1-3, C-1 201, 08034 Barcelona (Spain), eva.oller@upc.edu

Keywords: Shear strength, prestressed concrete, reinforced concrete, stirrups, mechanical model

INTRODUCTION

The strength of structural concrete members subjected to bending and shear is affected by the existing multi-axial state of stress, the anisotropy induced by diagonal concrete cracking, the bond between concrete and reinforcement and the brittle failure, among other phenomena. Furthermore, prestressing considerably modifies the stresses and strains fields, the cracking load and the crack patterns, affecting not only the structural response under service loads, but also the mode of failure and the ultimate capacity in comparison to reinforced concrete members.

In order to predict such a complex behavior, refined analytical and numerical models have been developed (Bairán and Marí 2006, 2007; Bentz 2000; Ferreira et al. 2013; Mohr et al. 2010; Navarro-Gregori et al. 2007; Petrangeli et al. 1999; Saritas and Filippou 2009; Vecchio and Collins 1986; Vecchio 2000). Particularly, it is possible to account among other aspects for crack-induced anisotropy, which brings in the migration of shear stresses through the cross-section as the cracks develop and the crack width grows. These models have contributed to better understand the evolution of the resisting mechanisms according the experimentally observed behavior.

The applicability of the aforementioned models in daily engineering practice, however, is still limited because of their complexity, time consumption and dependency on the numerous input parameters required. On the opposite, most simple equations used in practice are semi-empirical, without a clear mechanical meaning, present large scatter and bias when compared with databases of experimental results and cannot be easily adapted to the technical advances (new materials, external strengthening, etc.). Furthermore, empirical approaches make the application of performance-based-design difficult.

With the purpose of providing useful formulations for daily engineering practice, simplified models for the shear strength of RC and PC members, based on sound theories have been also developed. The most relevant among them, are those carried out by (Choi and Hong 2007; Collins et al. 2008; Muttoni and Fernández Ruiz 2008; Recupero et al. 2003; Reineck 1991; Tureyen and Frosch 2003; Wolf and Frosch 2007; Zararis and Papadakis, 2001), some of which have been included in structural design codes, such as the CSA A23.3-14 (2014) or the FIB Model Code (2013). On the contrary, other codes have incorporated empirical formulations, such as the ACI-318 Building Code (2011) and the Eurocode 2 (2002) for concrete structures, especially for beams without transverse reinforcement. Nevertheless, the shear strength of structural concrete members is still an open topic: as a matter of fact, no universally accepted simplified and accurate design formulation, which is capable to be adapted or extended to many different situations without the need for adjustments to existing or new experimental results, with similar levels of accuracy in all cases, is yet available.

For prestressed concrete members the debate is even more open, despite the extensive research carried out during more than six decades, oriented to identify the governing parameters, their influence on the shear strength and the failure modes. Relevant works were the early tests performed Zwoyer and Siess (1954), by Evans and Schumacher (1963), by Olesen et al. (1967), and by Kar (1968), on pre-tensioned concrete beams. Variables included in their studies were the level of prestressing (P/A), the longitudinal and shear reinforcement ratios, the shape of the cross section, the shear span a and the type of curing. Among the different modes of failure identified, Muguruma et al. (1983), studied the web crushing of prestressed concrete beams, the main variables being the ratio of yield force in the prestressed steel to yield force in the non-prestressed steel and the area of vertical stirrups. With respect to the concrete strength, Elzanaty et al. (1986) studied the shear capacity of prestressed concrete beams using high strength concrete and Choulli et al. (2008) tested high strength self-

compacting concrete beams. In both cases, a reduction of the shear strength was found with respect to that of conventional concrete, so that a limitation in the concrete compressive strength of about 65 MPa was recommended when computing the shear strength.

In order to assess existing post-tensioned concrete bridges, Rupf et al. (2013), tested post-tensioned I beams with drapped tendons and low amounts of shear reinforcement. They found that the shear strength and the failure mode of prestressed concrete girders are significantly influenced by the amount of shear reinforcement, the level of post-tensioning force, and the presence of flanges. De Silva et al. (2006), studied experimentally the influence of longitudinal and transverse reinforcement ratios, prestressing level and concrete strength on the crack width and spacing in partially prestressed concrete members.

Related to shear design models, Wolf and Frosch (2007) made relevant contributions proposing a simplified model based on the shear transfer capacity of the un-cracked concrete region, and including the contribution of the flanges in I beams. Park et al. (2013) extended their strain-based strength model to prestressed concrete structures by performing a layered analysis of the compressed zone. Zhang et al. (2014a, 2014b) developed a shear strength numerical model based on plasticity concepts, bond slip, crack widening and shear-flexure interaction. One of their conclusions was, as also reported by Marí et al. (2015), that the stirrups enhance the shear transfer capacity of the un-cracked concrete chord.

Furthermore, some aspects related to the shear behavior and shear strength are not clearly explained by the existing simplified formulations. Some examples are: the influence of the load level, of the amount of transverse reinforcement or of the presence of axial forces, on the concrete contribution, V_c; the contribution of the flanges in beams with T or I cross-section to the shear strength; the influence of the eccentricity of the post-tensioning tendons on the shear strength; and the reason why the shear strength is influenced by the longitudinal reinforcement and the position of the critical shear crack.

In order to answer these and other similar questions in daily engineering practice, simple but accurate models supported by a theory capable to capture the physics of the shear response are needed.

Recently, a mechanical model for the prediction of the shear strength of reinforced concrete beams with rectangular, I or T shaped sections, with or without transverse reinforcement, has been developed by Cladera et al. (2015) and Marí et al. (2015). The predictions of the model were compared with a large database of tests results on RC beams, already published by Reineck et al. (2013, 2014), showing small bias and dispersion. This model has also been extended to FRP reinforced concrete beams (Marí et al. 2014; Oller et al. 2015).

In this paper, the above mentioned shear model is generalized to the case of prestressed concrete members. For this purpose, the structural effects of prestressing on the shear response and on the different modes of failure are identified and accounted for in the derivation of the equations governing the model. The model predictions are compared with those of a large database of prestressed concrete beams with and without stirrups obtaining, in general, very good results. In addition, the influence of some relevant parameters on the shear response is studied and compared with the experimentally observed tendencies. A design example, based on a beam tested by Oh and Kim (2004), is fully developed to show the practical applicability of the model. Finally, conclusions are drawn about the capability of the model to provide rational explanations for the observed behavior.

MECHANISM OF SHEAR RESISTANCE

According to ASCE-ACI Committee 445 (1998), the shear strength in a slender RC beam is provided by: a) the shear resisted by the uncracked concrete chord; b) the friction and residual tensile forces developed along the crack; c) the shear strength provided by the transverse reinforcement; and d) the dowel action developed by the longitudinal

reinforcement. Under incremental loading, inclined flexural cracks develop along the web, forming the first branch of the critical crack (see Figs. 1 and 2). During a relatively large portion of the load history, a significant fraction of the shear force is transferred through the inclined cracks by means of aggregate interlock and residual tensile stresses, both produced by the bridging of stresses through the aggregates and the uncracked concrete at the meso-scale. However, while loading increases, the critical crack width increases, reducing the shear transferred along the crack. Then, a redistribution of shear stresses to the advantage of other resisting actions takes place, as is needed to satisfy the internal equilibrium conditions. In general, the shear stresses in the compression chord, which has remained uncracked during most part of the loading, tend to increase. Therefore, the compression chord will be subjected to a multi-axial stress state consisting in, at least, axial compression and shear.

Eventually, a new branch of the critical crack develops above the neutral axis trough the compression chord, at the point where the concrete strength under multiaxial stresses is first reached. At the same time, there is an increment of force in the longitudinal reinforcement due to inclined cracks in the web. Near the supports, this fact, joinly with the dowel action, may produce longitudinal bond cracks in the concrete in contact with the tensile flexural reinforcement. If premature bond failure does not take place, failure of the element will be controlled by the shear capacity of the compression chord as it is the last element that typically initiates softening, reducing its capacity as the crack propagates. Resistance of the compression chord is assumed in this work to be governed by Kupfer's biaxial failure envelope (Kupfer and Gerstle 1973) (Fig. 3), mainly in the compression-tension branch, when vertical compression stresses are negligible or small in comparison to longitudinal ones. This failure criterion is in accordance with that proposed by Zwoyer and Siess more than 60 years ago, when the concept that shear failures could be considered as a type of premature compression failure (Zwoyer and Siess 1954) was developed, and with the work of Kar in

prestressed concrete beams related to the internal stress redistribution and the strain concentration in the concrete chord (Kar 1968).

Prestressing introduces a set of self-balanced forces on concrete structures which modify the stresses, internal forces, strains, deflections and failure modes. The most important effects of prestressing on the shear response, which will be accounted for in the proposed model, are briefly recalled next.

In partially prestressed members, in which flexural cracks may develop at service under certain load combinations, a shear-flexure failure mechanism may take place, as it occurs in many reinforced concrete members. In such cases the cracks inclination, the neutral axis depth, the stress levels and, consequently, the shear transferred by the uncracked concrete chord and by the stirrups, are affected by the level of the prestressing force. Fig. 4 shows a prestressed specimen tested at TU Dortmund in the course of a research project funded by the German Federal Highway Research Institute (BASt) (Maurer et al. 2014). Initial flexural cracks appeared at P=700 kN, first shear-flexural cracks were observed at P=1200 KN and failure took place at P=1890 kN. It can be observed how the angle of inclination of the cracks near the centroid of the beam section is very small (about 22º), because the effect of the compressive stresses introduced by the prestressing force.

In totally prestressed members, mostly without shear reinforcement, inclined cracks may develop and propagate along the web, without the formation of flexural cracks, thus preventing the formation of a compression chord and the development of a flexure-shear resisting mechanism. In addition, in members with thin webs the compression stresses due to prestressing may increase the risk of concrete crushing. These two failure modes will be dealt with later in the paper. Finally, in the case of inclined tendons, the vertical component of the prestressing force, $V_p = P \cdot \sin\alpha$ reduces the external shear force.

DESCRIPTION OF THE MODEL

Basic assumptions

In the present model, it is considered that the total shear resistance, Eq. (1), is the sum of the shear resisted by concrete and by the transverse reinforcement (V_s). The concrete contribution is explicitly separated into the following components, whose importance is considered to be variable as damage propagates: shear resisted in the uncracked compression chord (V_c), shear transferred across web cracks (V_w) and the contribution of the longitudinal reinforcement (V_l). Note that here V_c represents the shear in the compression chord of the beam, not the total concrete contribution to shear.

$$V = V_c + V_w + V_l + V_s = f_{ct} \cdot b \cdot d \cdot \left(v_c + v_w + v_l + v_s \right) \tag{1}$$

Lower case variables v_c, v_w, v_l and v_s are the dimensionless values of the shear transfer actions and f_{ct} is the concrete tensile strength defined as given by Eq. (2), and not greater than 4.60 MPa, as for high-strength concrete the shear strength does not increase significantly due to the fracture of the aggregates (Cladera and Marí 2004, 2005).

$$f_{ct} = 0.30 \cdot \sqrt[3]{f'^{2}_{c}} \leq 4.60\ MPa \tag{2}$$

As the crack opens, the aggregate interlock and residual tension decrease, and an increase in the shear transferred by the compression concrete chord takes place. Hence, it will be assumed that at the limit state, previous to incipient failure, the shear stress distribution in the critical section is similar to the one represented in Fig. 5, where the approximated distribution of each contributing action is also indicated, c is the neutral axis depth and d the effective depth of the cross-section. Note that in Fig. 5, the stage just prior to the formation of the crack in the compression chord is considered. This stress profile is a qualitative distribution of the stresses in a section close to that of the tip of the first branch of the critical crack, and is not affected by the local state of stress around the crack tip.

194 In developing the design formulation, some additional simplifications are also
195 considered and described in the following.

196 ***Neutral axis depth***

197 Neutral axis depth (c) and height of uncracked zone are treated as equivalent, for design
198 purposes. Furthermore, in the case of shear failure prior to flexural yielding, longitudinal
199 reinforcement is assumed to remain in the elastic range. The distribution of normal
200 compressive stresses in the uncracked zone will be then considered linear; hence, the position
201 of the neutral axis can be computed as that of a cracked section in the elastic range. A
202 methodology to compute the neutral axis depth in prestressed concrete members is explained
203 next. Fig. 6 shows a typical cross section of a prestressed concrete beam subjected to a
204 bending moment M and a prestressing force P with an eccentricity e. To take into account the
205 contribution of the different types of reinforcement that may exist in the cross section (only
206 mild reinforcement, A_s, only active reinforcement, A_p, or both), the effective depth will be
207 defined as:

208 $$d = \frac{A_s d_s + A_p d_p}{A_s + A_p} \tag{3}$$

209 where d_s and d_p are the distances between the maximum compressed concrete fiber and the
210 centroid of the mild steel tensile reinforcement and the prestressing reinforcement placed in
211 the tensile zone of the cross-section, respectively.

212 In order to accurately calculate the neutral axis depth in a cracked prestressed concrete
213 section, the equilibrium equations between the internal forces (axial forces and bending
214 moments) and the stresses in the concrete and in the mild and prestressing reinforcements
215 must be solved, considering also the strain compatibility provided by the plane section
216 assumption. Due to the presence of the axial load, both equilibrium equations are coupled and,
217 as a consequence, the neutral axis depth depends on the mild and prestressing reinforcement

amounts, on the bending moment, on the prestressing force and on its eccentricity. Therefore, its computation is not straightforward, requiring an iterative procedure to solve the non-linear set of equations (Saqan and Rasheed 2011).

For practical purposes, it is proposed to obtain c by means of a linear interpolation between the neutral axis depth c_0 obtained for the same reinforcement amounts, considering P=0, and the total depth c=h, corresponding to the decompression prestressing force, i.e. the force applied at the considered eccentricity, which, in combination with an external moment M, produces zero stress at the most tensioned fiber (see Fig. 6). The interpolation equation for the relative neutral axis depth, c/d becomes:

$$\frac{c}{d} = \frac{c_0}{d} + \left(\frac{h}{d} - \frac{c_0}{d}\right)\left(\frac{d}{h}\right)\frac{Pk_t}{M - Pe} \tag{4}$$

where k_t= I_c/(A_c·v_{bot}) is the upper limit of the central kern, I_c and A_c are the second moment of inertia and the area of the cross section, respectively, and v_{bot} is the distance between the centroid and the most tensioned fiber of the section.

The neutral axis depth for P=0 (reinforced concrete) can be obtained by means of the following approximate expression:

$$\frac{c_0}{d} = n\rho_l\left(-1 + \sqrt{1 + \frac{2}{n\rho_l}}\right) \tag{5}$$

where ρ_l is the equivalent longitudinal tensile reinforcement ratio and n is the modular ratio. For members with mild steel reinforcement and tendons, $n\rho_l$ can be determined as follows:

$$n\rho_l = n_s\rho_s + n_p\rho_p \quad ; \quad n_s\rho_s = \frac{E_s}{E_c}\frac{A_s}{b{\cdot}d} \quad ; \quad n_p\rho_p = \frac{E_p}{E_c}\frac{A_p}{b{\cdot}d} \tag{6}$$

where b is the width of the cross-section, which is equal to the flexural effective compression flange width, for T or I-shaped sections; E_c is the secant modulus of elasticity of concrete according to Eurocode 2 (see Eq. (7)), and not greater than 39000 MPa for ULS shear calculations.

241 $$E_c = 22000\left(\frac{f_{cm}}{10}\right)^{0.3} \leq 39000\ MPa \quad (7)$$

242 As will be seen later, it is conservatively assumed in this model that the critical shear
243 crack develops from the last flexural crack, considering that the bending moment at ULS at
244 the initiation of the crack equals to the cracking moment. Therefore, when *M* is the cracking
245 moment in Eq. (4), it can be expressed as Eq. (8)

246 $$\frac{c}{d} = \frac{c_0}{d} + \left(\frac{h}{d} - \frac{c_0}{d}\right)\left(\frac{d}{h}\right)\frac{\sigma_{cp}}{\sigma_{cp} + f_{ct}} \quad (8)$$

247 where $\sigma_{cp}=P/A_c$ is the concrete compression stress at the centroid of the section produced
248 by the prestressing force. Eq. (8) has been compared with the theoretical solution by solving
249 the non-linear system of coupled equations, for a large number of cases covering different
250 levels of prestressing (σ_{cp}/f_{ct}), eccentricities (e/c) and non-prestressed neutral axis depth c_0,
251 obtaining good correlation for usual cases. Therefore, the straightforward Eq. (8) will be
252 adopted in this study to obtain c/*d* for prestressed elements.

253 ***Critical crack inclination***

254 Based on experimental and numerical observations of RC beams, the mean crack
255 inclination is approximated by a function of the relative neutral axis depth (c/d_s), by Eq. (9).

256 $$\cot\theta = \frac{0.85}{\left(1 - \frac{c}{d_s}\right)} = \frac{0.85 d_s}{(d_s - c)} \leq 2.5 \quad (9)$$

257 For the case of I or T shaped sections, there is a change of crack inclination in case that
258 the crack reaches the flanges, see Fig. 7. After parametric studies, however, it has been
259 observed that the influence of this fact on the shear strength is small so, for the sake of
260 simplicity, it will not be taken into account in the formulation, thus obtaining a slightly
261 conservative solution (Cladera et al. 2015).

The longitudinal normal stresses introduced by prestressing modify the angle of the principal stresses and, therefore, the angle of inclination of cracks. Since in prestressed concrete members the neutral axis depth increases, the change produced in the angle θ is automatically incorporated in the model by keeping the horizontal projection of the crack between its initiation and the neutral axis depth to $0.85 \cdot d_s$. The $\cot\theta$ of the critical shear crack angle for prestressed concrete members, given by Eq. (9) will be, therefore, higher than in reinforced concrete members without axial load. In prestressed members without longitudinal mild reinforcement (A_s=0), $\cot\theta$ can be computed adopting $d_s = d_p$ in Eq (9).

Position of the critical crack

In the present model, the weakest section in front of a combined shear-bending failure is considered to be placed at the tip of the first branch of the critical crack for beams with constant geometry and reinforcement (Fig. 8). Any other section closer to the zero bending moment point has a larger depth of the compression chord, produced by the inclination of the crack, and will resist a larger shear force. Any other section placed farther from the support will have the same depth of the compression chord, but will be subjected to higher normal stresses and, therefore, will have a larger shear transfer capacity.

When the load is increasingly applied, flexural cracks successively appear as the bending moment increases. The crack spacing depends basically on tensile concrete and bond properties (Fig. 9). It is assumed that the critical crack is the closest crack to the zero bending moment point and that it starts where the bending moment diagram at failure reaches the cracking moment of the section. As a result, $s_{cr} = M_{cr}/V_u$, which is a conservative assumption.

In prestressed concrete, the increment of cracking moment modifies the position where the critical crack initiates and the position of the critical section, which are displaced farther from the zero bending moment point than in RC structures (Fig. 9). Thus, the bending

moment at the critical section increases and, consequently, also the shear resisted by the compressed concrete chord.

Vertical concrete stresses produced by transverse reinforcement

When stirrups are anchored in the compression zone, they contribute to the strength of the compression chord by producing a confining vertical compression (σ_y) at a depth larger than the concrete cover (d'), see Fig. 10, of value given by Eq. (10):

$$\sigma_y = \frac{A_{sw} f_{yw}}{b} = \rho_w f_{yw} = \frac{v_s f_{ct}}{0.85} \tag{10}$$

where v_s is the dimensionless contribution of the transverse reinforcement to the shear strength, given by Eq. (11).

Contribution of transverse reinforcement (V_s)

The contribution of shear reinforcement, Eq. (11) is taken as the sum of the forces in the stirrups that intersect the inclined crack up to a height of (d_s-c), as shown in Fig. 5, and assuming that the transverse reinforcement is yielded along the entire crack height.

$$v_s = \frac{V_s}{f_{ct} \cdot b \cdot d} = \frac{0.85 d_s A_{sw} \cdot f_{yw}}{f_{ct} \cdot b \cdot d} \tag{11}$$

Contribution of cracked concrete web (V_w)

The shear resistance of cracked concrete in the web is considered as the residual tensile stress of cracked concrete. The mean tensile stress of the stress-strain curve is considered distributed along the depth c_w of the cracked zone of the cross-section where the tensile σ-ε curve reaches zero tension, see Fig. 11. A linear softening branch of the σ-ε curve has been assumed, which is consistently dependent on the fracture energy in mode I (G_f).

By enforcing the compliance between the crack opening at the level of the longitudinal reinforcement and at the point of the crack where the residual tensile stress is zero, and relating the crack opening to the reinforcement longitudinal strain ε_s and the crack spacing, the shear transferred along the closest part of the crack can be expressed as a function of ε_s. At

ULS a strain in the reinforcement close to 0.0009 has been assumed, resulting the same expression for reinforced concrete and prestressed concrete members to simplify the calculation procedure, see Eq. (12). The complete derivation of this equation can be found in Marí et al. (2015).

$$v_w = \frac{V_w}{f_{ct} \cdot b \cdot d} = 167 \frac{f_{ct}}{E_c} \frac{b_w}{b} \left(1 + \frac{2 \cdot G_f \cdot E_c}{f_{ct}^2 \cdot d_0} \right) \quad (12)$$

where b_w and b are the web and the flange widths, respectively; f_{ct} is the concrete tensile strength evaluated as the mean tensile strength according to Eurocode 2 (2002), but limiting the concrete compression strength to 60 MPa in order to account for the possible fracture of the aggregate in high-strength concrete; G_f is the fracture energy of concrete, which depends on the concrete strength and the aggregate size, computed as shown in Eq. (13) (Marí et al. 2015); and d_0 is the effective depth, d, but not lesser than 100 mm.

$$G_f = 0.028 \cdot f_{cm}^{0.18} \cdot d_{\max}^{0.32} \quad (13)$$

where f_{cm} is the mean concrete compressive strength and d_{max} is the maximum aggregate size.

In the case of T- or I-shaped sections, it is accepted that the shear transferred along the crack takes place mainly in the web, so the web width b_w has been used in Eq. (12) when computing v_w.

Contribution of the longitudinal reinforcement (Dowel action, V_l)

Contribution of longitudinal reinforcement, or dowel action, is considered by the model only when there are stirrups, as they provide a constraint to the vertical movement of the longitudinal bars, enabling them to transfer shear. In the case of prestressed concrete members, only mild reinforcement or prestressing bars supported by the stirrups are considered to produce dowel action. In order to evaluate such contribution, it is considered that the longitudinal bars are doubly fixed at the two stirrups adjacent to the crack, and subjected to bending due to a relative imposed displacement between the two extremities.

This relative vertical displacement is caused by the opening of the critical crack and by the shear deformation of the compression chord. This contribution clearly depends on the tensile steel ratio, that is implicitly represented by means of *c*/*d*. A simplified expression is presented in Eq. (14). A more detailed derivation of the equation is carried out in Marí et al. (2015).

$$v_s > 0 \Rightarrow \quad v_l = \frac{V_l}{f_{ct} \cdot b \cdot d} \approx 0.23 \cdot \frac{n\rho_l}{1 - \frac{c}{d}} \tag{14}$$

Contribution of the compression chord (V_c)

As previously mentioned, the shear transferred by the compression chord starts softening when the most stressed fiber reaches Kupfer's failure envelope. The stresses at any point of the uncracked zone are obtained assuming a linear distribution of longitudinal flexural stresses and a constant transversal confining stresses provided by the existing stirrups. The position of the failure point depends on the ratio between bending moment and shear force (*M*/*Vd*) at the considered critical section. A study performed by Marí et al. (2015) shows that for values of *M*/*Vd* less than 3 (which is usually the position of the critical shear section), the point where failure initiates is placed at a distance from the neutral axis around λ=0.425*c*, being *c* the depth of the compressed zone.

By means of a Mohr's circle analysis, the shear stress τ_λ at the point where failure initiates, can be related to the principal and normal stresses by Eq. (15)

$$\tau_\lambda = \sigma_1 \sqrt{1 - \frac{\sigma_x + \sigma_y}{\sigma_1} + \frac{\sigma_x \cdot \sigma_y}{\sigma_1^2}} \tag{15}$$

Once the value of the shear stress at three points is known, $\tau(0)=0$, $\tau(c)=0$ and $\tau(\lambda)=\tau_\lambda$, the equation for the assumed parabolic shear stress distribution (Fig. 5) is obtained and, by integration, the shear force transferred by the compression chord is derived, Eq. (16):

$$V_c = \int_0^c \tau(y) \cdot b \cdot dy \quad ; \quad v_c = \frac{V_c}{f_{ct}\, b\, d} = \zeta K_\lambda R_t \frac{c}{d} \frac{b_{v,eff}}{b} \sqrt{1 - \frac{\sigma_x + \sigma_y}{\sigma_1} + \frac{\sigma_x \cdot \sigma_y}{\sigma_1^2}} \tag{16}$$

where σ_x is the normal stress in the most stressed fiber, located at a distance $\lambda \cdot c$ from the neutral axis; $K\lambda$ is a parameter relating the mean shear stress in the compression chord with the shear stress in the most stressed fiber, and $b_{v,eff}$ is an effective width, to take into account that for T or I sections the shear stresses along the depth of the compression chord are concentrated in the portion of the flanges near the web:

$$c \le h_f \quad b_{v,eff} = b_v = b_w + 2h_f \le b \tag{17a}$$

$$c > h_f \quad b_{v,eff} = b_v \eta + b_w (1-\eta) \quad ; \quad \eta = 3\left(\frac{h_f}{c}\right)^2 - 2\left(\frac{h_f}{c}\right)^3 \tag{17b}$$

where b and b_w are the width of the flange and the web respectively; h_f is the flange depth, as defined in Fig. 6. The neutral axis depth c must be calculated accounting for the geometry of the T or I section, as is proposed in Cladera et al (2015). For rectangular sections, $b=b_w$ and $b_{v,eff}/b=1$.

In order to obtain the concrete contribution to the shear strength in PC members, the prestressing force, with its inclination and eccentricity, must be included in the equilibrium of forces and moments. Fig 12 shows the internal forces acting on a portion of beam placed over the critical shear crack.

ΔP in Fig. 12 is the increment of force in the active reinforcement due to the crack opening, which will be neglected in this work assuming in a simplified manner the same shear strength for members with bonded and unbonded tendons. Then, the equilibrium equations are:

$$C = T + V_w \tan\theta + P\cos\alpha \tag{18}$$

$$V = V_c + V_w + V_l + V_s + P\sin\alpha \tag{19}$$

$$C \cdot z_s = M_{Ed} + V_c\, 0.85 d_s + V_w \beta_w d_s + 0.425 \cdot V_s d_s + P\left(d_s - d_p\right)\cos\alpha \tag{20}$$

where equilibrium of moments is taken with respect to the point where the crack is crossed by the longitudinal reinforcement.

The compressive normal stress at the failure point of the concrete chord (at a distance λc from the neutral axis) is given by:

$$\sigma_x = \frac{2\lambda C}{bc} = \frac{2\lambda\left(M_{Ed} + P\left(d_s - d_p\right)\cos\alpha + V_c\, 0.85 d_s + V_w z_w\, d_s + 0.425 \cdot V_s\, d_s\right)}{b\, c\,(d_s - \frac{c}{3})} \tag{21}$$

The confining stresses (σ_y) are given by Eq. (10) as a function of the contribution of the transverse reinforcement, v_s, (Eq. 11) as $\sigma_{cy} = f_{ct}\, v_s /0.85$.

By setting the equilibrium equations between the internal forces and the stress resultants, shown in Fig. 12, Eq. (16) can be rewritten as

$$v_c = \zeta K_\lambda R_t \frac{c}{d}\frac{b_{v,eff}}{b}\sqrt{1 - \frac{2\lambda\left(\mu\frac{d}{d_s} + \mu_p\frac{d}{d_s} + 0.85 v_c + v_w z_w + 0.425 v_s\right)}{\frac{c}{d}\left(1 - \frac{c}{3d_s}\right)R_t}\left(\frac{v_s}{0.85R_t} - 1\right)} - \frac{v_s}{0.85R_t} \tag{22}$$

where μ is the non-dimensional moment at shear failure at the crack initiation given by Eq. (23) (Fig. 9); μ_P is the non-dimensional moment with respect to the mild reinforcement, due to prestressing given by Eq. (24); z_w is the lever arm of v_w with respect to point A (Fig. 12) (a conservative value of z_w=0.425d can be adopted without much error, since both v_w and the extension of residual stresses along the crack, at failure, are usually small); ζ is the parameter accounting for size effect in the compression chord, which can be assimilated to that of a splitting test, as proposed by Zararis and Papadakis (2001), and can be computed by Eq. (25).

$$\mu = \frac{M_{Ed}}{f_{ct} b d^2} \tag{23}$$

$$\mu_p = \frac{P\cos\alpha\,(d_s - d_p)}{f_{ct} b d^2} \tag{24}$$

$$\zeta = 1.2 - 0.2\,a \geq 0.65 \quad (a \text{ in meters}) \tag{25}$$

It is observed that v_c depends on v_s and that Eq. (22) is a recurrent equation, since R_t (strength reduction factor due to the biaxial stress state) is not known a priori; hence, in general, an iterative procedure is required to find v_c. After solving Eq. (22), however, it was found that v_c is almost a linear function of c/d, so for practical purposes, Eq. (26) is proposed as a linearization of Eq. (22).

$$v_c = \zeta \left\{ \left[0.88 + \left(0.20 + 0.50 \ \frac{b}{b_w} \right) v_s \right] \frac{c}{d} + 0.02 \right\} \frac{b_{v,eff}}{b} \left[0.94 + 0.3(\mu + \mu_p) \right] \quad (26)$$

Term 0.94+0.3(μ+μ_p) of Eq. (26) accounts for the influence of the bending moment on the concrete contribution, V_c. Adopting, as a conservative assumption, that the bending moment at shear failure is equal to the cracking moment, given by Eq. (27)

$$\mu = \mu_{cr} = \frac{1}{f_{ct} b d^2} \left[\frac{I_c f_{ct}}{y_t} + P\left(e + k_t\right) \right] \quad (27)$$

taking into account that d_p=v_{top}+e (see Fig. 12) and after some mathematical arrangements, Eq. (26) becomes:

$$v_c = \zeta \left\{ \left(0.88 + \left(0.20 + 0.50 \frac{b}{b_w} \right) v_s \right) \frac{c}{d} + 0.02 \right\} \frac{b_{v,eff}}{b} \left[1 + 0.3 \frac{P \cos\alpha \, (c + d_s - d_p)}{f_{ct} b d^2} \right] \quad (28)$$

The right bracket in Eq. (28) will be called K_p, a factor which takes into account the higher cracking moment in a prestressed concrete section, with respect to a reinforced concrete section. In case of reinforced concrete, P=0, the non-dimensional cracking moment (Eq. 27) becomes μ_{cr}=0.2 and term 0.94+0.3(μ+μ_p) becomes equal to 1.

Shear failure in regions without flexural cracks

In case of highly prestressed simply supported concrete beams, such as some T or I beams, with minimum or no shear reinforcement, no flexural cracks take place near the supports even at high loading levels. In these regions, the beam web (usually thin) is subjected to high shear stresses produced by the applied shear force, combined with normal

compressive stresses produced by prestressing, generating a biaxial compression-tension state of stress. When, at the most stressed point of the web, see Fig. 13, the principal stresses reach the biaxial failure envelope, (see Fig. 3), a diagonal crack develops through the entire beam height (Fig. 14). It has been experimentally observed that the cracking load turns out to be almost equal to the ultimate load (Evans and Schumacher 1963; Elzanaty et al. 1986); because of the eccentricity of prestressing, the top compression stresses are not capable to control the diagonal crack propagation (see Fig. 14).

According to Mohr's circle of stresses, the shear producing the principal stress σ_1 at the beam centroid is:

$$V_u = \frac{I_c b_w}{S_c}\sigma_1\sqrt{1+\alpha_l\frac{\sigma_{cp}}{\sigma_1}} = \frac{I_c b_w}{S_c}R_t f_{ct}\sqrt{1+\alpha_l\frac{\sigma_{cp}}{R_t f_{ct}}} \tag{29}$$

where I_c is the second moment of area, S_c is the first moment of the area above and about the centroid, α_l is the factor which takes into account the portion of prestressing force transferred to concrete at the considered section, which is ≤ 1.0 for pretensioned tendons, and is equal to 1.0 for other types of prestressing, σ_{cp} is the concrete compressive stress at the centroid axis due to prestressing and R_t is a tensile strength reduction factor due to the biaxial stress state, given by

$$\sigma_1 = \left(1-0.8\frac{\sigma_2}{f_{cc}}\right)f_{ct} = R_t f_{ct} \tag{30}$$

Usually R_t ranges from 0.77 to 0.95, so a value of R_t = 0.8 outside the square root and R_t= 1 inside the square root will be conservatively adopted.

In the case of beams with shear reinforcement, once the web cracks, stirrups start working and a shear force higher than the cracking shear can be resisted, as observed by Elzanaty et al. (1986). As a consequence, higher bending moments take place near the supports which, in most cases, produce flexural cracks. Therefore, in beams with transverse

443 reinforcement, the shear strength will be calculated accepting flexural cracks, by means of the
444 model previously described in the previous sections which will provide a lower bound value.

445 ***Concrete compression crushing in regions with shear cracks***

446 The beam failure may be governed by the concrete struts in beams with shear
447 reinforcement and relatively thin webs. In this case, the concrete diagonals would crush prior
448 to the yielding of the transverse reinforcement, resulting in a brittle failure (Aparicio et al.
449 1998; Rangan 1991). To check the maximum capacity of the struts, Eq. (31), this proposal
450 adopts the same formulation of the current Eurocode 2 (2002), with the angle of the
451 compression strut given by Eq. (9):

452 $$V_{Rd,\max} = \alpha_{cw} b_w d_s \nu_1 f_c^{'} \frac{\cot\theta}{1+\cot^2\theta} \quad (31)$$

453 where ν_1 is a strength reduction factor for concrete cracked in shear, taking into account the
454 transversal tensile stresses. The values given by Eq. (32) are adopted:

455 $$\nu_1 = 0.6 \quad for \quad f_c^{'} \le 60\ MPa \quad (32a)$$

456 $$\nu_1 = 0.9 - f_c^{'}/200 \quad for \quad f_c^{'} > 60\ MPa \quad (32b)$$

457 and α_{cw} is a coefficient taking account the state of stress in the struts, Eq. (33)

458 $$\alpha_{cw} = 1 \qquad for\ non-prestressed\ structures \quad (33a)$$

459 $$\alpha_{cw} = 1 + \sigma_{cp}/f_c^{'} \qquad for\ 0 \le \sigma_{cp} \le 0.25 f_c^{'} \quad (33b)$$

460 $$\alpha_{cw} = 1.25 \qquad for\ 0.25 f_c^{'} \le \sigma_{cp} \le 0.50 f_c^{'} \quad (33c)$$

461 $$\alpha_{cw} = 2.5\left(1-\sigma_{cp}/f_c^{'}\right) \qquad for\ 0.5 f_c^{'} \le \sigma_{cp} \le f_c^{'} \quad (33d)$$

462 ***Summary of the steps following the proposed general model***

463 The described model provides the contribution of each shear transfer action to the global
464 shear strength. In summary, to obtain the shear strength or to calculate the stirrups needed, it
465 is necessary to use Eq. (1) for the total shear strength, and Eqs. (11), (12), (14) and (28) for

the different non-dimensional contributions. Moreover, to calculate the neutral axis depth, Eq. (5) shall be used for RC structures. For prestressed elements, Eq. (8) is needed to obtain *c*/d taking into account the stress due to prestressing. Finally, the effective width of the concrete chord, in case of beams with I or T cross-sections, is computed by Eq. (17). Additionally, the maximum shear strength given by the struts should be checked, according to Eqs. (31)-(33).

SIMPLIFIED EQUATIONS IN A CODE-TYPE FORMAT

For design purposes, some simplifications are still necessary in order to make the model easier to use in daily engineering practice. Taking into account that when shear-flexure failure takes place, both the aggregate interlock and the dowel action are small compared to the shear resisted by the uncracked zone, v_w and v_l have been incorporated into v_c. For this purpose, the following average values have been adopted: v_w=0.035, v_l=0.025, v_s=0.25 and c/d=0.35. Then, term (v_w+0.02)/0.35=0.157 has been added to 0.88 and the dowel action term $v_l/(0.35\cdot 0.25)$, which only exists when $A_{st}>0$, has been added to the factor multiplying v_s in Eq. (28), resulting in the following compact equation:

$$V_{cu} = \zeta \frac{c}{d} K_p \left[0.30 \frac{f_c'^{2/3}}{\gamma_c} + 0.5 \left(1 + \frac{b}{b_w} \right) \frac{V_s}{bd} \right] b_{v,eff} d \qquad (34)$$

where the design tensile strength of concrete, f_{ctd}, is expressed in terms of the concrete compressive strength, f'_c, reduced by the corresponding partial safety coefficient, and K_p is the factor which takes into account the effects of prestressing, whose value is:

$$K_p = 1 + 0.24 \frac{P \cdot y_t}{f_{ct} b d^2} \qquad (35)$$

where y_t is the distance from the centroid of the section to the most stressed fiber in tension. In Eq. (35) a coefficient 0.24 has been used in spite of the original value of 0.30 (right parenthesis in Eq. 26), to take into account that the neutral axis depth in prestressed concrete sections (see Eqs. 5 to 8) is higher than the one assumed (c/d=0.35) to merge the different components into a single concrete contribution V_{cu}.

As previously discussed (see Fig. 9), in the case of prestressed elements, the flexural cracking is displaced farther away form the support axis with respect to a similar element with $P = 0$. Consequently, the control cross-section also moves accordingly. To take this fact into account, in design, shear strength shall be checked at least at a distance $s_{cr} = d_s(1+0.4\sigma_{cp}/f_{ct})$ from the support axis, where $\sigma_{cp} = P/A_c$ is the mean concrete normal stress due to prestressing.

Then, the shear strength verification can be carried out as follows:

$$V_{Ed} = V_{Ed0} - P\sin\alpha \le V_u = V_{cu} + V_{su} \quad \textit{or} \text{ alternatively} \quad V_{Ed} \le V_u = V_{cu} + V_{su} + P\sin\alpha \tag{36}$$

where $V_{Ed,0}$ is the design shear force acting at the control section, V_{cu} is given by Eq. (29) and V_{su} is:

$$V_{su} = \left(d_s - c\right)\cot\theta \cdot \frac{A_{sw}}{s_t} f_{ywd} \tag{37}$$

where θ is the mean crack inclination given by Eq. (9).

Shear reinforcement is necessary when the shear design force exceeds the shear resisted by the concrete, without transverse reinforcement, V_{cu0}.

$$V_{cu0} = 0.30 \frac{f_c'^{2/3}}{\gamma_c} \zeta \frac{c}{d} K_p b_{v,eff} d \tag{38}$$

In that case, the required strength contribution provided by the shear reinforcement is given by Eq. (39), and the area of shear reinforcement will be obtained using Eq. (37).

$$V_{su} = \frac{V_{Ed} - V_{cu0}}{1 + 0.5\zeta \frac{c}{d} K_p \left(1 + \frac{b}{b_w}\right) \frac{b_{v,eff}}{b}} \tag{39}$$

It is observed that due to the confinement of the uncracked concrete zone produced by the stirrups, the amount of transverse reinforcement is reduced, as the denominator in Eq. (39) is always larger than 1.

VERIFICATION OF THE MODEL WITH SHEAR TESTS RESULTS

The four complete databases developed by ACI-DafStb for reinforced and prestressed concrete beams (Reineck et al. 2013, 2014; ACI-DAfStb 617, 2015) have been used to verify the proposed model and to compare its predictions with those of three current international codes ACI318.11 (2011), CSA A23.3-14 (2014) and Eurocode 2 (2002). The results are shown in Table 1 and in Fig. 15. All beams included in the four databases have been used for this evaluation. The ranges of the variables for the different tests included in the databases are presented in Table 2. All explicit partial safety factors have been removed from the original formulations. Moreover, the mean value of the materials strength has been used for all calculations. Therefore, the predictions compared are not exactly the real predictions of the different models as f_{ck} or f'_c values should be used depending on the formulation employed.

As can be seen in Table 1 and Fig. 15, the proposed model, both in its general or simplified formulations, correlates better with the results of the four databases than any of the three considered code formulations. Summing up, for the 1285 tested beams, the average of the V_{test}/V_{pred} ratio, parameter directly related to accuracy, is 1.04 for the general equations and 1.14 for the simplified equations. For the ACI318-11 provisions the ratio equals 1.44, 1.26 for EC2 and 1.33 for CSA A23.3-14. The coefficient of variation, a measure of precision, is clearly lower for the proposed models than for the current codes of practice. The two most precise models for the four databases are the general model (CoV = 18.4%) and the simplified model (CoV = 19.3%). For ACI318-04 and EC-2 predictions, the CoV is very close to 35%, almost doubling the CoV of the general model. For CSA A23.3-14 the CoV equals 26.9%. As observed in Table 1, with respect to the current codes of practice, the CSA A23.3-14 is the one that provides least scatter for the four groups of beams.

The predictions obtained by means of the proposed formulation and the three codes considered are compared in Fig. 16 with some selected series of tests extracted from the ACI-

DafStb databases for prestressed elements (De Silva et al. 2006; Elzanaty et al. 1986; Muguruma et al. 1983; Olesen et al. 1967). In Fig. 16 the influence of the following parameters is shown: the compression stresses due to prestressing for beams without stirrups (Fig. 16a); the concrete compression strength for beams without stirrups (Fig. 16b); the influence of the amount of stirrups in I-beams (Fig. 16c); and the influence of the slenderness, *a/d*, for I-beams with stirrups (Fig. 16d). It is clearly shown that the proposed equations follow the trends given by the tested beams in all studied situations. It must be highlighted that the proposed model predicts higher shear strength for 3 out of 4 test series shown in Figure 16. For the 3 experimental tests by Elzanaty et al. (1986) shown in Figure 16b the predicted shear strength by EC-2 is unconservatively larger than the strength predicted by the model proposed in this paper. In fact, these 3 beams collapsed due to strut crushing. The model proposed uses the same equations than EC-2 for this type of collapse, as previously commented, but the angle of the concrete struts is fixed in this model.

APPLICATION EXAMPLE

The shear strength of a simply supported post-tensioned I-shaped bridge girder tested by Oh and Kim (2004) (girder 1) is predicted using the proposed code format simplified equations. The beam has a total length of 10.6 m, a span length of 10 m, a total height 1.20 m and is subjected to a concentrated load placed at 3.6 m of the right support and 6.4 m of the left support. The cross-section dimensions and reinforcement arrangements are shown in Fig. 17. For calculation purposes, the top and bottom flanges have been considered constant in depth, resulting: b_{ftop}=800 mm, h_{ftop}=175 mm, b_w=180 mm, h_w=850 mm, b_{fbot}=600 mm, h_{fbot}= 175mm. The bottom longitudinal reinforcement consists of 16 bars of 19.1 mm diameter (A_s =4584.3 mm^2, effective depth d_s = 1100 mm). No safety coefficients are used since the objective is to predict the experimental ultimate load (P_u=2303 kN).

The beam is post-tensioned with three tendons of parabolic layout, each composed by 6

seven-wire strands, with a nominal diameter of 98.71 mm^2 ($A_{p,tendon}$ = 6x98.71=592.3 mm^2), placed inside a 50 mm diameter sheath, subsequently injected with cement grout. The equivalent tendon has a steel area $A_{p,tot}$=3x592.3=1776.8 mm^2 and a parabolic layout with zero eccentricities at the support axes and a maximum eccentricity of 410 mm at the center span (see Figure 17), resulting Eq. 40, where s is the distance to the support (in m):

$$e(s) = 0.052 + 0.188s - 0.0188s^2; \quad e'(s) = 0.0376(5 - s) \tag{40}$$

The tendon is stressed from both ends and the prestressing force after losses, which can be considered constant along the whole tendon length, is P =1790.8 kN (σ_{cp} =1007.9 N/mm^2).

The stirrups, of 12.9 mm nominal diameter, are double legged with a loop extending out of the web of the girder. The stirrups spacing was 200 mm (A_{sw}/s_t = 1.307 mm^2/mm) at the right hand side and 400mm (A_{sw}/s_t = 0.653 mm^2/mm) at the left hand side.

Concrete was made with 19 mm crushed granite aggregate. The compressive strength (obtained from 100 x 200 cylinder tests at the time of shear testing) was f_{cm} = 42.8 MPa, the tensile strength f_{ct} = 3.67 MPa and the modulus of elasticity E_c =34000 MPa. Yield strength and ultimate strengths of longitudinal and stirrup bars were 345 MPa and 540 MPa, respectively, obtained from tests in the laboratory. Ultimate and yield strengths of prestressing steel were f_{pmax} = 1860 MPa and f_{py} =1670 MPa; and E_p = 195000 MPa.

Gross section characteristics: area A_c=0.398 m^2, first moment of inertia S_c=0.0903 m^3; second moment of inertia I_c = 0.01046 m^4, and the distances from the c.o.g to the most compressed and tensile fibers are, respectively, y_c = 0.555m, y_t= - 0.645m.

The distance from the control section to the support axis is:

$$\sigma_{cp} = \frac{P}{A_c} = \frac{1790816}{398000} = 4.5\ MPa \quad ; \quad s_{cr} = d_s\left(1 + 0.4\frac{\sigma_{cp}}{f_{ct}}\right) = 1639\ mm \tag{41}$$

The critical section will be placed in the short span, since the shear force is higher and an arch effect is not expected because a/d > 2.5.

The eccentricity and slope of the equivalent tendon at the control section (s_{cr} =1639 mm), obtained from Eq. (40), are e = 0.309m and e' = 0.126. The effective depth of the tendon at such section is d_p =e+ y_c= 864 mm.

Preliminary calculations, using Eqs. (3) and (5):

$$n=\frac{E_s}{E_c}=5.88;\quad n_p=\frac{E_p}{E_c}=5.73;\quad d=\frac{d_s A_s+d_p A_p}{A_s+A_p}=1035mm;\quad b=b_{ftop}=800mm \tag{42}$$

$$\rho_s=\frac{A_s}{b\cdot d}=0.00554\quad;\quad \rho_p=\frac{A_p}{b\cdot d}=0.00364\quad;\quad n\rho_l=n_s\rho_s+n_p\rho_p=0.05343 \tag{43}$$

$$\frac{c_0}{d}=n\rho_l\left(-1+\sqrt{1+\frac{2}{n\rho_l}}\right)=0.278;\quad c_0=287mm \tag{44}$$

Neutral axis depth including the prestressing effects (Eq. 8):

$$\frac{c}{d}=\frac{c_0}{d}+\left(\frac{h}{d}-\frac{c_0}{d}\right)\left(\frac{d}{h}\right)\frac{\sigma_{cp}}{\sigma_{cp}+f_{ct}}= \\ =0.278+0.8\left(\frac{1200}{1031}-0.278\right)\frac{1031}{1200}\frac{4.5}{4.5+3.67}=0.613\,;\, c=634\,mm>h_f \tag{45}$$

The shear span of the right hand side is a=3.6 m, and the size effect (Eq. 25) factor results to be:

$$\zeta=1.2-0.2a=1.2-0.2\cdot 3.6\geq 0.65\Rightarrow\zeta=0.65 \tag{46}$$

The effective shear width (Eq. 17), taking into account that $c>h_f$, *($h_f/c=0.276$)* is:

$$b_v=b_w+2h_f=530\,;\,\eta=3\left(\frac{h_f}{c}\right)^2-2\left(\frac{h_f}{c}\right)^3=0.186\,;\,b_{v,eff}=b_v\eta+b_w\left(1-\eta\right)=245mm \tag{47}$$

Prestressing factor (Eq. 35):

$$K_p=1+0.24\frac{P\cdot y_t}{f_{ct}\cdot b\cdot d^2}=1+0.24\frac{1790816\cdot 645}{3.67\cdot 800\cdot 1035^2}=1.088 \tag{48}$$

Angle of inclination of the struts (Eq. 9):

$$\cot\theta=\frac{0.85\cdot d_s}{d_s-c}=\frac{0.85\cdot 1100}{1100-634}=2.00\leq 2.5\quad;\quad\theta=26.5^{\circ} \tag{49}$$

602 Shear resisted by the stirrups at the short shear span (Eq. 37):

603 $$V_{su} = \left(d_s - c\right)\cot\theta \cdot \frac{A_{sw}}{s_t} f_{ywd} = 0{,}85 \cdot d_s \frac{A_{sw}}{s_t} f_{ywd} = 0{,}85 \cdot 100 \cdot 1.307 \cdot 540 = 659904N \quad (50)$$

604 The shear resisted by the concrete (Eq. 34), including the confinement of the stirrups, is:

605 $$V_{cu} = \zeta \frac{c}{d} K_p \left[0.30 \frac{f_c'^{2/3}}{\gamma_c} + 0.5 \left(1 + \frac{b}{b_w} \right) \frac{V_s}{bd} \right] b_{v,eff} d = \quad (51)$$
$$= 0.65 \cdot 0.613 \cdot 1.088 \left[3.65 + 0.5 \left(1 + \frac{800}{180} \right) \frac{659904}{800 \cdot 1035} \right] 245 \cdot 1035 = 639735N$$

606 Vertical component of the prestressing force at the control section:

607 $$V_p = P \sin\alpha = 1790816 \cdot 0.1256 = 224926N \quad (52)$$

608 Total shear resisted (Eq. 36), at the critical section, including the prestressing
609 contribution V_p:

610 $$V_u = V_{cu} + V_{su} + V_p = 639735 + 659904 + 224922 = 1524561N \quad (53)$$

611 Part of the shear is due to the beam's self weight V_g. Therefore, the shear caused by the
612 applied point load which can be resisted ($V_{u,q}$) is:

613 $$V_{u,q} = V_u - V_g = 1524561 - g\left(\frac{l}{2} - s_{cr}\right) = 1524561 - 9.95\left(5000 - 1639\right) = 1491119N \quad (54)$$

614 and the load which produces such shear is $Q = V_{uq}/0.64$=2330 kN, which is 1.1 % higher than
615 the load resisted by the tested girder 1 (2303 kN).

616 The maximum shear that can be resisted (the shear producing crushing of the web, Eq.
617 (31) is:

618 $$V_{rd,\max} = \alpha_{cw} b_w d_s \nu_1 f_c' \frac{\cot\theta + \cot\alpha}{1 + \cot^2\theta} = 0.6 \cdot 155 \cdot 1100 \cdot 1.105 \cdot 42.8 \frac{2}{1 + 2^2} = 1931084N > V_u \quad (55)$$

619 Where α_{cv} =0.6, ν_1 =1+σ_{cp}/f_c'=1.105 and b_w=180-0.5·50=155 mm (50 mm diameter
620 grouted sheath). Therefore, shear-flexure takes place, for a concentrated load of Q_u = 2330 kN

Oh and Kim (2004) tested a second beam (girder 2) identical to girder 1 except that its concrete compressive strength was 62.1 MPa in spite of 42.8 MPa. The ultimate load obtained for girder 2 was 2312 kN, which was practically the same than girder 1 (2302 kN), even though the compressive strength of girder 2 was almost 50% higher.

Repeating all calculations for girder 2, using the code format equations proposed in this paper, the following results are obtained: f_{ct} =4.60 MPa, σ_{cp}=4.50 MPa, σ_{cp}/f_{ctm}=0.978, s_{cr}=1531 mm, d=1031mm, $\alpha\rho$=0.0478, $\cot\theta$=1.83, c/d=0.571, $b_{v,eff}$=254.4 mm, $\sin\alpha$=0.13, V_{su}=659.9 kN, V_{cu}=702.0 kN, $P\sin\alpha$=232.3kN, $V_u = V_{cu}+V_{su}+P\cdot\sin\alpha$=1594.2 kN, V_{uq}=1559.7 kN and Q_u=2434kN, that is 5.4% higher than the experimental value and only 4.6% higher than the ultimate load computed with the model for girder 1. Such a small difference is due to several reasons:

1) The concrete contribution to shear strength depends on the tensile strength $f_{ct}=0.3f'^{2/3}_c$, rather than on the compressive strength. Thus, increasing the compressive strength from 42.8 to 62.1 MPa, and provided that f'_c must be limited to 60 MPa, results in an increment of 24.9 % of the tensile strength.

2) If f_{ct} increases, the relative compressive stress introduced by prestressing σ_{cp}/f_{ct} decreases, resulting in a reduction of c/d from 0.613 to 0.571 (6.9% smaller).

3) The contribution of the stirrups V_{su} is independent of f'_c, since the horizontal projection of the first branch of the critical crack is constant and equal to $0.85d_s$

4) The vertical concrete stresses due to confinement provided by the stirrups, given by term $0.5\left(1+\frac{b}{b_w}\right)\frac{V_s}{bd}$ in Eq. (34), are comparable to the concrete tensile strength and, therefore, the influence of f'_c on V_{cu} becomes diluted.

CONCLUSIONS

The following conclusions can be drawn from the model capacities and results:

1. A general model has been developed for the prediction of the shear-flexural strength of reinforced and prestressed concrete members with and without transverse reinforcement, with I, T or rectangular cross sections, which explicitly accounts for the most significant shear transfer actions. The expressions obtained can be particularized for reinforced concrete members, rectangular sections and sections without transverse reinforcement in a straightforward manner.

2. After some justified simplifications, simple and direct expressions that include the most relevant parameters governing the structural behavior, have been derived. The proposed formulae are valid both for design of the transverse reinforcement and for assessment, without the need of performing iterations.

3. The prestressing force increases the shear strength of the compressed concrete chord by increasing the neutral axis depth, the cracking moment and the normal stresses. These effects have been incorporated into the model.

4. A simple expression to obtain the neutral axis depth in prestressed concrete sections cracked in bending has been derived, which results very useful for computing the shear strength of prestressed concrete members.

5. It is assumed by the model that the critical crack initiates at the section where the bending moment, at failure, equals the cracking moment. Therefore, the critical crack in PC members is farther from the zero bending moment point than in RC members.

6. The predictions of the present model are in very good agreement with the experimental results of the four ACI-DAfStb databases consisting of 1285 shear tests on slender reinforced and prestressed concrete beams with and without stirrups. Summing up, for the 1285 tested beams, the average of the V_{test}/V_{pred} ratio is 1.04 for the general equations and 1.14 for the simplified equations. For the ACI318-11 provisions the ratio equals 1.44, 1.26 for EC2 and 1.33 for CSA A23.3-14. The CoV is 18.4% for the general model and 19.3% for the

simplified model. For ACI318-04, EC-2 and CSA A23.3-14 the CoV equals 35.4%, 34.5% and 26.9% respectively. This fact indicates that the proposed model exhibits less scattering and is more accurate than the provisions of the current codes. Moreover, according to the studies of tendency made, the model predicts very well the experimentally observed influence of the different parameters involved.

7. The ultimate capacity of two simply supported post-tensioned I beams tested by Oh and Kim (2004) has been computed in detail, to show the practical applicability of the model. The ultimate capacities predicted by the model are very similar to those experimentally measured (V_{pred}/V_{exp}=1.01 and 1.05 for girders 1 and 2, respectively). The model is capable of capturing the small influence of an increment in the value of f'_c on the shear strength.

ACKNOWLEDGEMENTS

The present work has been developed under the framework of research projects BIA2012-36848, BIA2012-31432, funded by the Spanish Ministry of Economy and Competitiveness (MINECO) and the Europeans Funds for Regional Development (ERDF), and under the financial help of Infraestructures de Catalunya (ICAT).

REFERENCES

ACI-Committee-318. (2011). *Building Code Requirements of Structural Concrete and Commentary. 2011*. ACI.

ACI-DAfStb 617. (2015). *ACI-DAfStb databases 2015 on shear tests for evaluating relationships for the shear design of structural concrete members without and with stirrups.* (K.-H. Reineck & D. Dunkelberg, Eds.). Berlin: Beuth Verl.

Aparicio, A. C., Calavera, J., & del Pozo, F. (1998). Ensayos de esfuerzo cortante por agotamiento de las bielas comprimidas con Hormigón de Altas Prestaciones. In *Primer Symposium Nacional de Hormigón de Altas Prestaciones* (pp. 469–482).

ASCE-American Concrete Institute (ACI) Committee-445. (1998). Recent approaches to shear design of structural concrete. *Journal of Structural Engineering*, *124*(2), 1375–1417.

Bairán, J. M., & Marí, A. R. (2006). Coupled model for the non-linear analysis of anisotropic sections subjected to general 3D loading. Part 1: Theoretical formulation. *Computers and Structures*, *84*(31-32), 2254–2263. doi:10.1016/j.compstruc.2006.08.036

Bairán, J. M., & Marí, A. R. (2007). Multiaxial-coupled analysis of RC cross-sections subjected to combined forces. *Engineering Structures*, *29*(8), 1722–1738. doi:10.1016/j.engstruct.2006.09.007

Bentz, E. C. (2000). *Sectional analysis of reinforced concrete members*. *Sectional analysis of reinforced concrete members*. University of Toronto.

Choi, K.-K., & Hong-Gun, P. (2007). Unified Shear Strength Model for Reinforced Concrete Beams-Part II: Verification and Simplified Method. *ACI Structural Journal*, *104*(2), 153–166.

Choulli, Y., Marí, A., & Cladera, A. (2008). Shear behaviour of full-scale prestressed i-beams made with self compacting concrete. *Materials and Structures*, *41*, 131–141.

Cladera, A., & Marí, A. R. (2004). Shear design procedure for reinforced normal and high-strength concrete beams using artificial neural networks. Part I: Beams without stirrups. *Engineering Structures*, *26*(7), 917–926. doi:10.1016/j.engstruct.2004.02.010

Cladera, A., & Marí, A. R. (2005). Experimental study on high-strength concrete beams failing in shear. *Engineering Structures*, *27*(10), 1519–1527. doi:10.1016/j.engstruct.2005.04.010

Cladera, A., Marí, A., Ribas, C., Bairán, J., & Oller, E. (2015). Predicting the shear–flexural strength of slender reinforced concrete T and I shaped beams. *Engineering Structures*, *101*, 386–398. doi:10.1016/j.engstruct.2015.07.025

Collins, M. P., Bentz, E. C., Sherwood, E. G., & Xie, L. (2008). An adequate theory for the shear strength of reinforced concrete structures. *Magazine of Concrete Research*, *60*(9), 635–650.

CSA group. (2014). *A23.3-14 Design of concrete structures* (June 2014.). Mississauga.

De Silva, S. ., Mutsuyoshi, H. ., Witchukreangkrai, E. ., & Takagi, M. (2006). Experimental Study on Shear Cracking Behaviour in I-shaped Partially Prestressed Concrete Beams. *Transactions of the Japan Concrete Institute*, *28*(2), 817–822.

Elzanaty, A. H., Nilson, A. H., & Slate, F. O. (1986a). Shear Capacity of Prestressed Concrete Beams Shear Capacity of Prestressed Concrete Beams Using High-Strength Concrete. *ACI Journal*, *83*(3), 359–368. doi:10.14359/10436

Elzanaty, A. H., Nilson, A. H., & Slate, F. O. (1986b). Shear Capacity of Prestressed Concrete Beams Using High-Strength Concrete. *ACI Journal*, *83*(3), 359–368. doi:10.14359/10436

European Committee for Standardization. (2002). *Eurocode 2: Design of Concrete Structures: Part 1: General Rules and Rules for Buildings*. European Committee for Standardization.

Evans, R. H., & Schumacher, E. G. (1963). Shear Strength of Prestressed Beams Without Web Reinforcement. *ACI Journal Proceedings*, *60*(11), 1621–1642. doi:10.14359/7907

Fédération Internationale du Béton. (2013). *fib Model Code for Concrete Structures 2010* (Vol. 1). Ernst & Sohn.

Ferreira, D., Bairán, J., & Marí, A. (2013). Numerical simulation of shear-strengthened RC beams. *Engineering Structures*, *46*, 359–374. doi:10.1016/j.engstruct.2012.06.050

Kar, J. N. (1968). Diagonal Cracking in Prestressed Concrete Beams. *Journal of the Structural Division - American Society of Civil Engineers*, *94*(1), 83–110.

Kupfer, H. B., & Gerstle, K. H. (1973). Behavior of concrete under biaxial stresses. *Journal of the Engineering Mechanics Division*, *99*(4), 853–866.

Marí, A., Bairán, J., Cladera, A., Oller, E., & Ribas, C. (2015). Shear-flexural strength mechanical model for the design and assessment of reinforced concrete beams. *Structure and Infrastructure Engineering*, *11*(11), 1399–1419. doi:10.1080/15732479.2014.964735

Marí, A., Cladera, A., Oller, E., & Bairán, J. (2014). Shear design of FRP reinforced concrete beams without transverse reinforcement. *Composites Part B: Engineering*, *57*, 228–241. doi:10.1016/j.compositesb.2013.10.005

Maurer, R., Gleich, P., Zilch, K., & Dunkelberg, D. (2014). Experimental investigations on the shear load bearing capacity of a large two-span prestressed concrete beam (In German). *Beton- Und Stahlbetonbau*, *109*(10), 654–665. doi:10.1002/best.201400054

Mohr, S., Bairán, J. M., & Marí, A. R. (2010). A frame element model for the analysis of reinforced concrete structures under shear and bending. *Engineering Structures*, *32*(12), 3936–3954. doi:10.1016/j.engstruct.2010.09.005

Muguruma, A. ., Watanabe, F. ., & Fujii, M. (1983). Experimental Study on Shear Resisting Behavior of Prestressed Reinforced Concrete Beams (in Japanese). *Transactions of the Japan Concrete Institute*, *5*, 453–456.

Muttoni, A., & Ruiz, M. F. (2008). Shear strength of members without transverse reinforcement as function of critical shear crack width. *ACI Structural Journal*, *105*(2), 163–172.

Navarro-Gregori, J., Miguel-Sosa, P., Fernández-Prada, M. A., & Filippou, F. C. (2007). A 3D numerical model for reinforced and prestressed concrete elements subjected to combined axial, bending, shear and torsion loading. *Engineering Structures*, *29*(12), 3404–3419. doi:10.1016/j.engstruct.2007.09.001

769 Oh, B. H., & Kim, K. S. (2004). Shear Behavior of Full-Scale Post-Tensioned Prestressed
770 Concrete Bridge Girders. *ACI Structural Journal*, *101*(2), 176–182.

771 Olesen, S. O. ., Sozen, M. A. ., & Siess, C. . (1967). Investigation of prestressed reinforced
772 concrete for highway bridges, part IV: Strength in shear of beams with web
773 reinforcement. *University of Illinois, College of Engineering, Bulletin 493*, *64*(134).

774 Oller, E., Marí, A., Bairán, J. M., & Cladera, A. (2015). Shear design of reinforced concrete
775 beams with FRP longitudinal and transverse reinforcement. *Composites Part B:*
776 *Engineering*, *74*, 104–122. doi:10.1016/j.compositesb.2014.12.031

777 Park, H.-G., Kang, S., & Choi, K.-K. (2013). Analytical model for shear strength of ordinary
778 and prestressed concrete beams. *Engineering Structures*, *46*, 94–103.
779 doi:10.1016/j.engstruct.2012.07.015

780 Petrangeli, M., Pinto, P. E., & Ciampi, V. (1999). Fiber element for cyclic bending and shear
781 of RC structures. I: Theory. *Journal of Engineering Mechanics*, *125*(9), 994–1001.
782 doi:10.1061/(ASCE)0733-9399(1999)125:9(994)

783 Rangan, V. B. (1991). Web crushing strength of reinforced and prestressed concrete beams.
784 *ACI Structural Journal*, *88*(1), 12–16. doi:10.14359/3050

785 Recupero, A., D'Aveni, A., & Ghersi, A. (2003). N-M-V interaction domains for box and I-
786 shaped reinforced concrete members. *ACI Structural Journal*, *100*(1), 113–119.
787 doi:10.14359/12445

788 Reineck, K. H. (1991). Ultimate shear force of structural concrete members without
789 transverse reinforcement derived from a mechanical model. *ACI Structural Journal*,
790 *88*(5), 592–602.

791 Reineck, K. H., Bentz, E. C., Fitik, B., Kuchma, D. A., & Bayrak, O. (2013). ACI-DafStb
792 database of shear tests on slender reinforced concrete beams without stirrups. *ACI*
793 *Structural Journal*, *110*(5).

794 Reineck, K.-H., Bentz, E., Fitik, B., Kuchma, D. A., & Bayrak, O. (2014). ACI-DAfStb
795 Databases for Shear Tests on Slender Reinforced Concrete Beams with Stirrups. *ACI*
796 *Structural Journal*, *111*(5), 1147–1156.

797 Rupf, M., Fernández Ruiz, M., & Muttoni, A. (2013). Post-tensioned girders with low
798 amounts of shear reinforcement: Shear strength and influence of flanges. *Engineering*
799 *Structures*, *56*, 357–371. doi:10.1016/j.engstruct.2013.05.024

800 Saqan, E., & Rasheed, H. (2011). Simplified nonlinear analysis to compute neutral axis depth
801 in prestressed concrete rectangular beams. *Journal of the Franklin Institute*, *348*(7),
802 1588–1604. doi:10.1016/j.jfranklin.2010.09.005

803 Saritas, A., & Filippou, F. C. (2009). Inelastic axial-flexure-shear coupling in a mixed
804 formulation beam finite element. *International Journal of Non-Linear Mechanics*, *44*(8),
805 913–922. doi:10.1016/j.ijnonlinmec.2009.06.007

Tureyen, A. K., & Frosch, R. J. (2003). Concrete Shear Strength: Another Perspective. *ACI Structural Journal*, *100*(5), 609–615.

Vecchio, F. J. (2000). Disturbed stress field model for reinforced concrete: formulation. *Journal of Structural Engineering*, *126*(9), 1070–1077.

Vecchio, F. J., & Collins, M. P. (1986). The modified compression-field theory for reinforced concrete elements subjected to shear. *ACI J.*, *83*(2), 219–231.

Wolf, T. S., & Frosch, R. J. (2007). Shear design of prestressed concrete: A unified approach. *Journal of Structural Engineering*, *133*(11), 1512–1519. doi:10.1061/(ASCE)0733-9445(2007)133:11(1512)

Zararis, P. D., & Papadakis, G. C. (2001). Diagonal shear failure and size effect in RC beams without web reinforcement. *Journal of Structural Engineering*, *127*(7), 733–742. doi:10.1061/(ASCE)0733-9445(2001)127:7(733)

Zhang, T., Visintin, P., Oehlers, D. J., & Griffith, M. C. (2014a). Presliding Shear Failure in Prestressed RC Beams. I: Partial-Interaction Mechanism. *Journal of Structural Engineering*, *140*(10), 04014069. doi:10.1061/(ASCE)ST.1943-541X.0000988

Zhang, T., Visintin, P., Oehlers, D. J., & Griffith, M. C. (2014b). Presliding Shear Failure in Prestressed RC Beams. II: Behavior. *Journal of Structural Engineering*, *140*(10), 04014070. doi:10.1061/(ASCE)ST.1943-541X.0000984

Zwoyer, E. M., & Siess, C. P. (1954). Ultimate Strength in Shear of Simply-Supported Prestressed Concrete Beams Without Web Reinforcement. *ACI Journal Proceedings*, *51*(10), 181–200. doi:10.14359/11673

Table 1. Verification of the proposed model for different databases: mean value and Coefficient of Variation (%) for V_{test}/V_{pred} ratio.

Database original source	Comments	No. beams	General eqs. (Eq. 1)		Simplified eqs. (Eq. 30)		ACI318-11		EC-2		CSA A23.3-14	
			Mean	CoV	Mean	CoV	Mean	CoV	Mean	CoV	Mean	CoV
(Reineck et al. 2013)	RC beams w/o stirrups	784	1.04	18.9	1.16	18.9	1.42	38.3	1.10	27.9	1.22	22.3
(Reineck et al. 2014)	RC beams with stirrups	170	1.05	17.0	1.12	16.5	1.52	25.8	1.44	29.6	1.29	17.9
(ACI-DAfStb 617 2015)	PC beams w/o stirrups	214	1.02	19.6	1.10	22.6	1.52	35.1	1.56	29.8	1.68	29.8
(ACI-DAfStb 617 2015)	PC beams with stirrups	117	1.05	15.1	1.05	16.1	1.28	20.5	1.54	37.2	1.40	16.2
All	All	1285	1.04	18.4	1.14	19.3	1.44	35.4	1.26	34.5	1.33	26.9

Table 2. Range of variables in the used databases.

Database	No. beams	b (mm)		b_w (mm)		d (mm) – Eq.3		a/d		f_c (MPa)		$n\rho$ Eq. 6		$\rho_w f_{yw}$ (MPa)		σ_{cp} (MPa)		V_{test} (kN)	
		min	max	min	max	min	max	min	max	min	max	min	max	min	max	min	max	min	max
RC beams w/o stirrups	784	50	3005	50	3005	57	3000	2.4	8.1	13	139	0.009	0.36	0	0	0	0	7	1308
RC beams with stirrups	170	110	1500	64	457	161	1369	2.4	7.1	13	125	0.008	0.28	0.28	24.4	0	0	81	3384
PC beams w/o stirrups	214	79	700	50	373	109	1025	2.4	7.4	15	105	0.008	0.25	0	0	0.17	14.8	18	721
PC beams with stirrups	117	150	1450	40	300	162	1363	2.5	6.9	18	102	0.006	0.19	0.23	17.5	0.34	17.3	41	3827

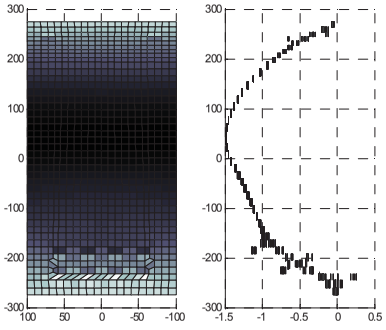
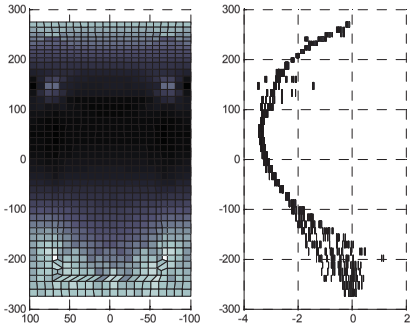
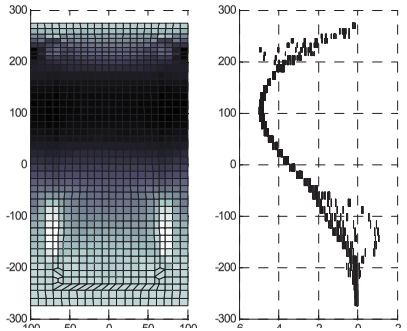

Figure 3

Click here to download Figure Figure 3.tif

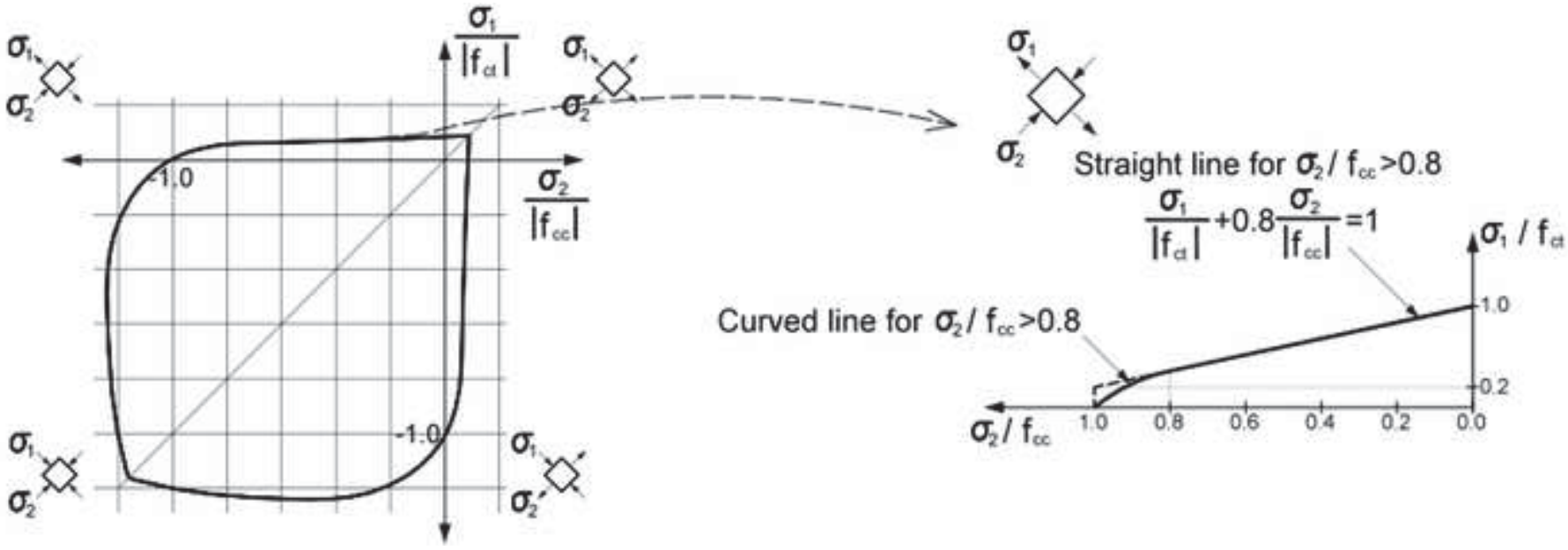

Figure 4a

Click here to download Figure Figure 4a.tif

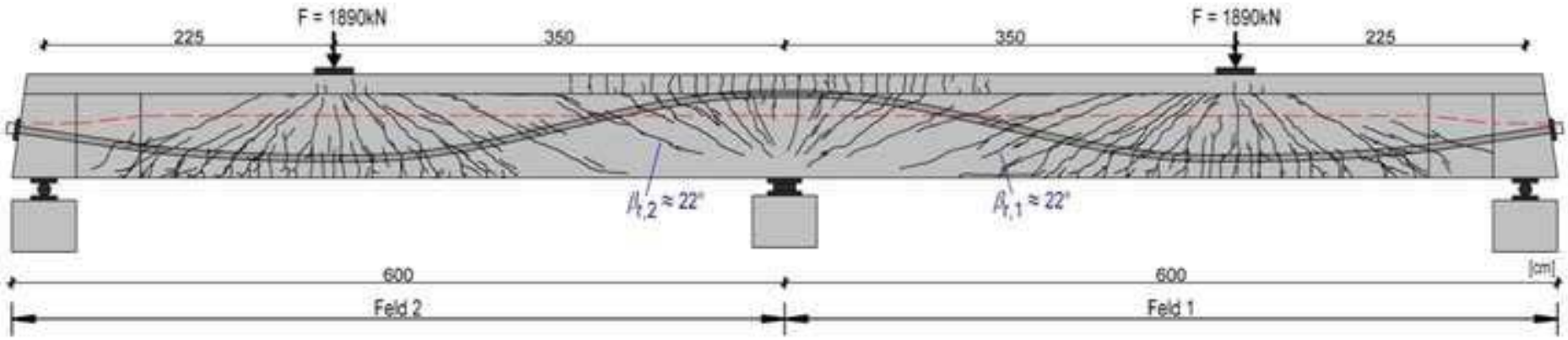

Figure 4b

Click here to download Figure Figure 4b.tif

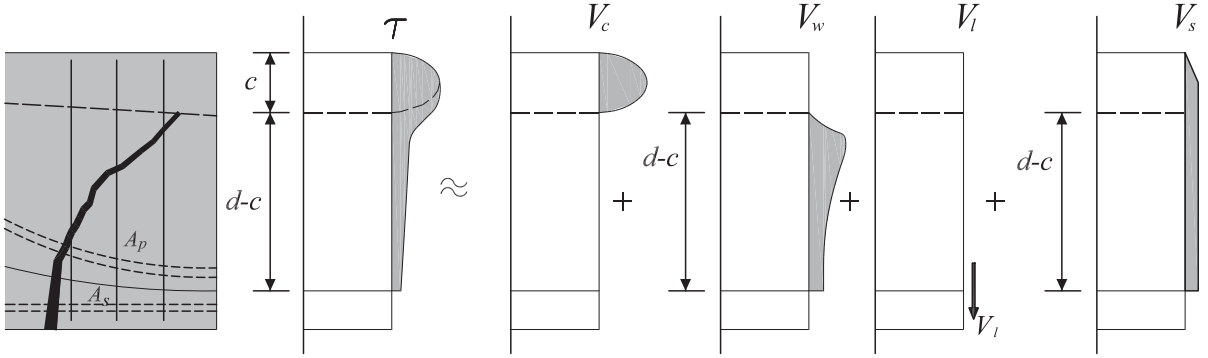
τ
c
d-c
A_p
A_s
≈
V_c
+
V_w
d-c
+
V_l
+
V_l
V_s
d-c

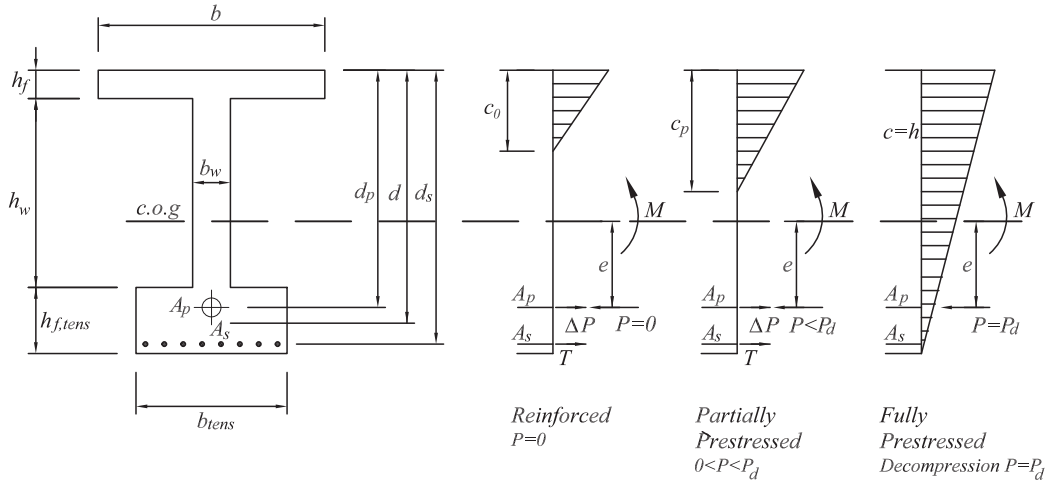
b
h_f
h_w
b_w
c.o.g
d_p
d
d_s
A_p
A_s
$h_{f,tens}$
b_{tens}
c_0
M
e
A_p
A_s
ΔP
P=0
T
Reinforced
P=0
c_p
M
e
A_p
A_s
ΔP
P<P_d
T
Partially
Prestressed
0<P<P_d
c=h
M
e
A_p
A_s
P=P_d
Fully
Prestressed
Decompression P=P_d

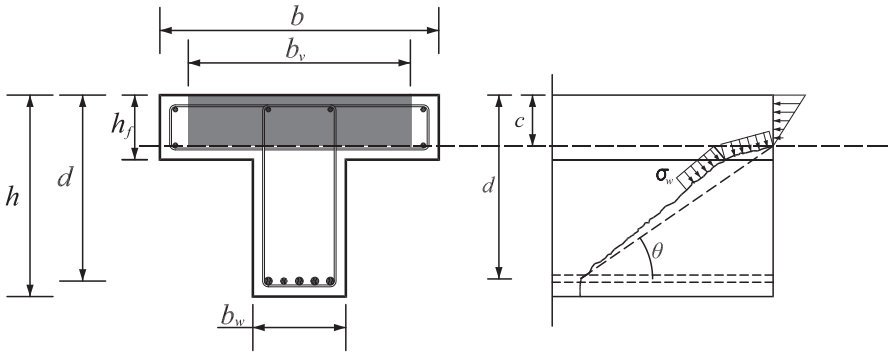
b
b_v
h_f
h
d
b_w
c
d
σ_w
θ

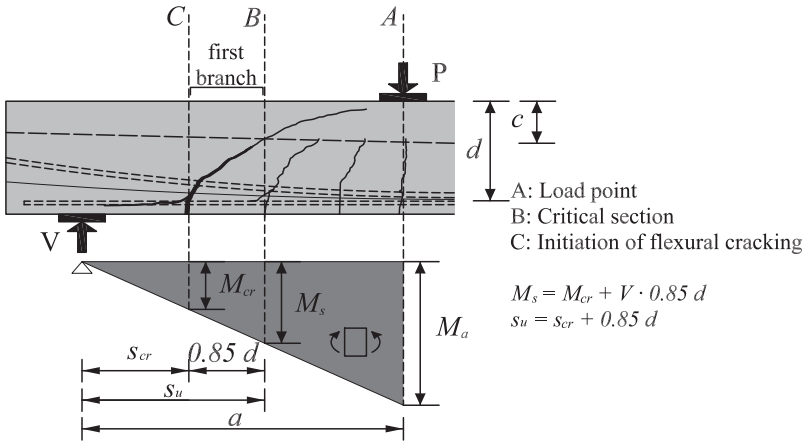
C
B
A
first
branch
P
c
d
V
M_{cr}
M_s
M_a
s_{cr}
0.85 d
s_u
a
A: Load point
B: Critical section
C: Initiation of flexural cracking
$M_s = M_{cr} + V \cdot 0.85\ d$
$s_u = s_{cr} + 0.85\ d$

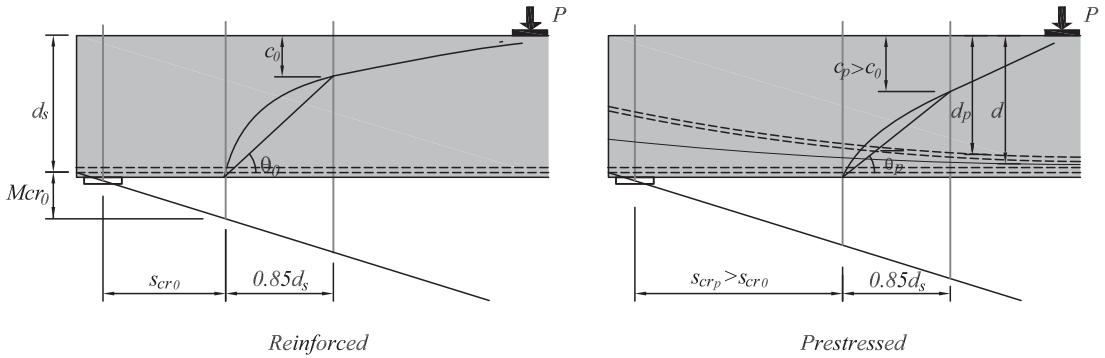
P
c_0
d_s
θ_0
Mcr_0
s_{cr0}
$0.85d_s$
Reinforced
P
$c_p > c_0$
d_p
d
θ_p
$s_{crp} > s_{cr0}$
$0.85d_s$
Prestressed

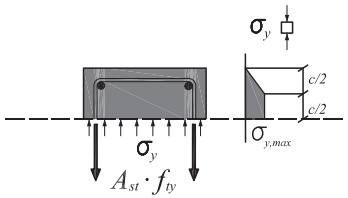
σy
c/2
c/2
σy,max
σy
Ast · fty

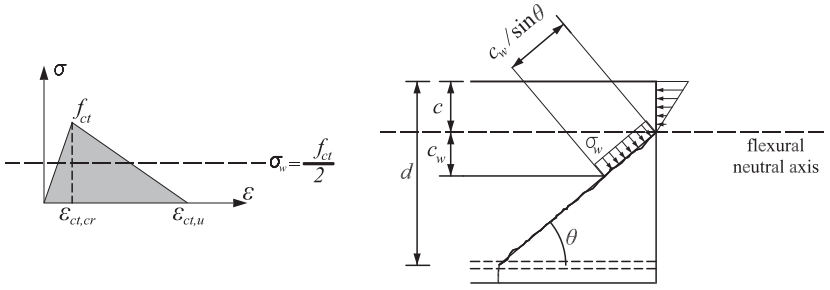
σ
f_{ct}
$\sigma_w = \frac{f_{ct}}{2}$
ε
$\varepsilon_{ct,cr}$
$\varepsilon_{ct,u}$
$c_w / \sin\theta$
c
c_w
d
σ_w
flexural
neutral axis
θ

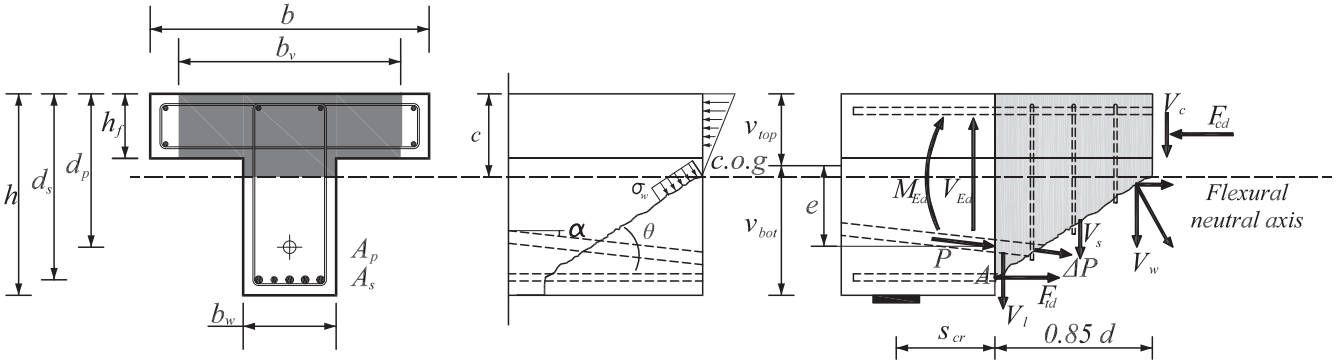
b
b_v
h_f
h
d_s
d_p
A_p
A_s
b_w
c
σ_w
α
θ
v_{top}
c.o.g
v_{bot}
e
M_{Ed}
V_{Ed}
P
ΔP
A
V_s
V_w
V_c
E_{cd}
E_{td}
V_l
Flexural
neutral axis
s_{cr}
0.85 d

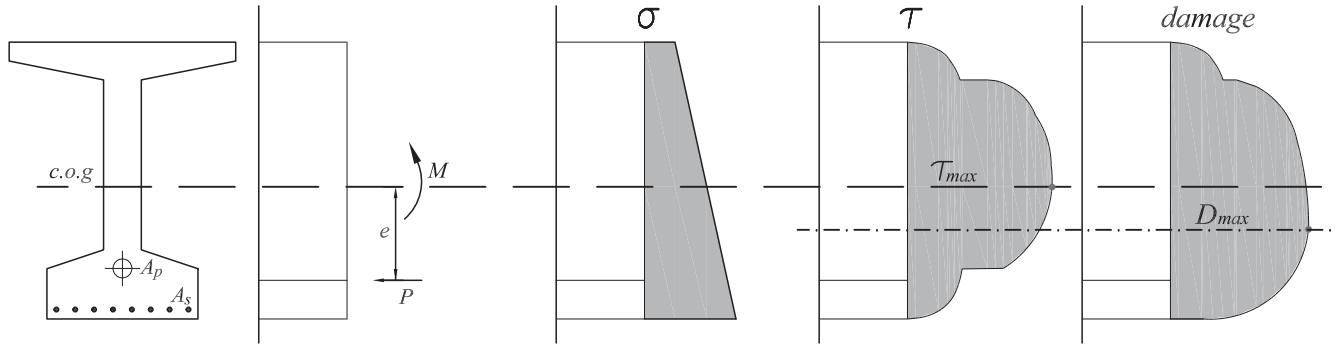
c.o.g
M
e
P
A_p
A_s
σ
τ
τ_{max}
damage
D_{max}

Figure 14

Click here to download Figure Figure 14.tif

Figure 15a

Click here to download Figure Figure 15a.pdf

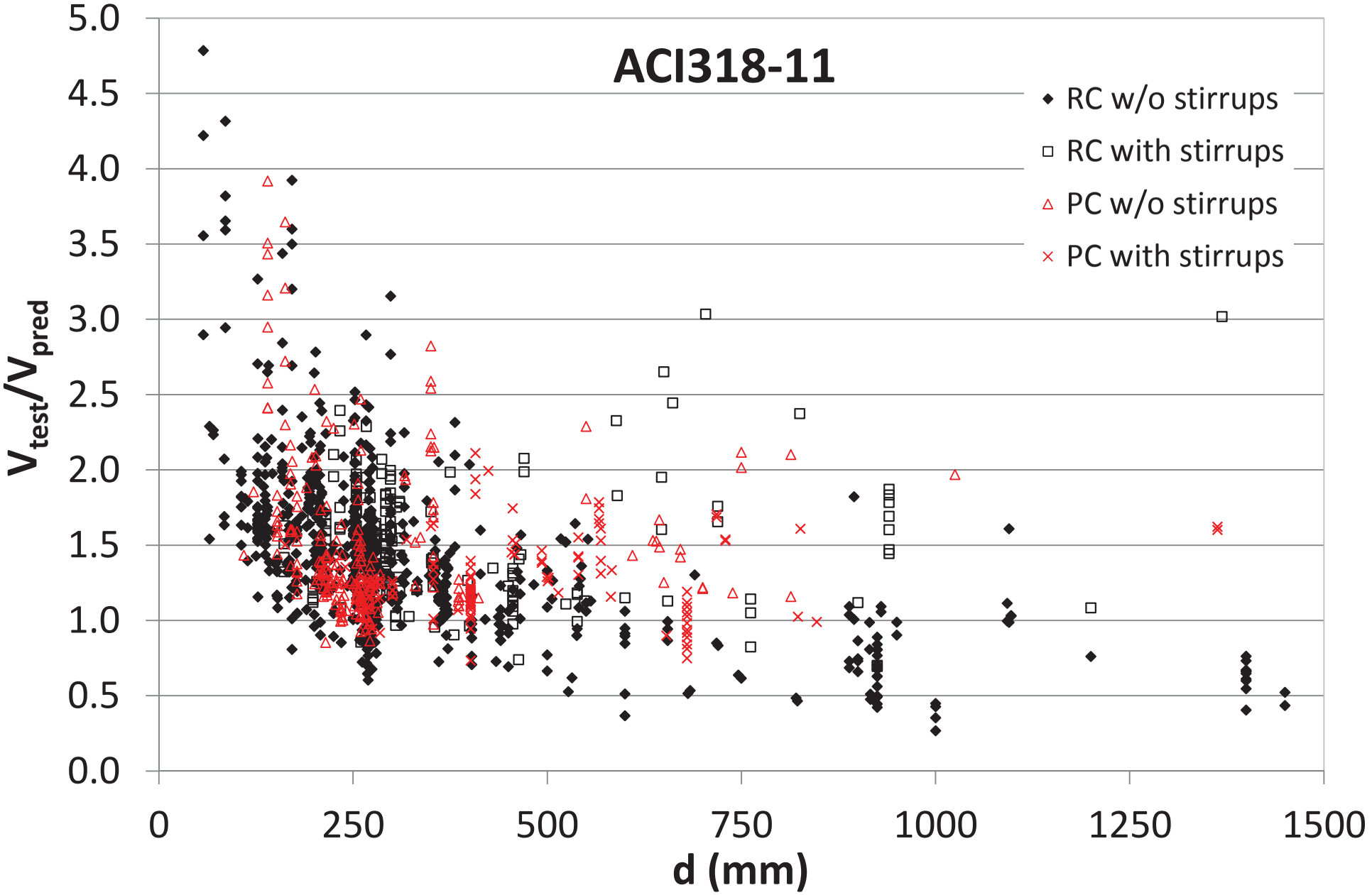

Figure 15b

Click here to download Figure Figure 15b.pdf

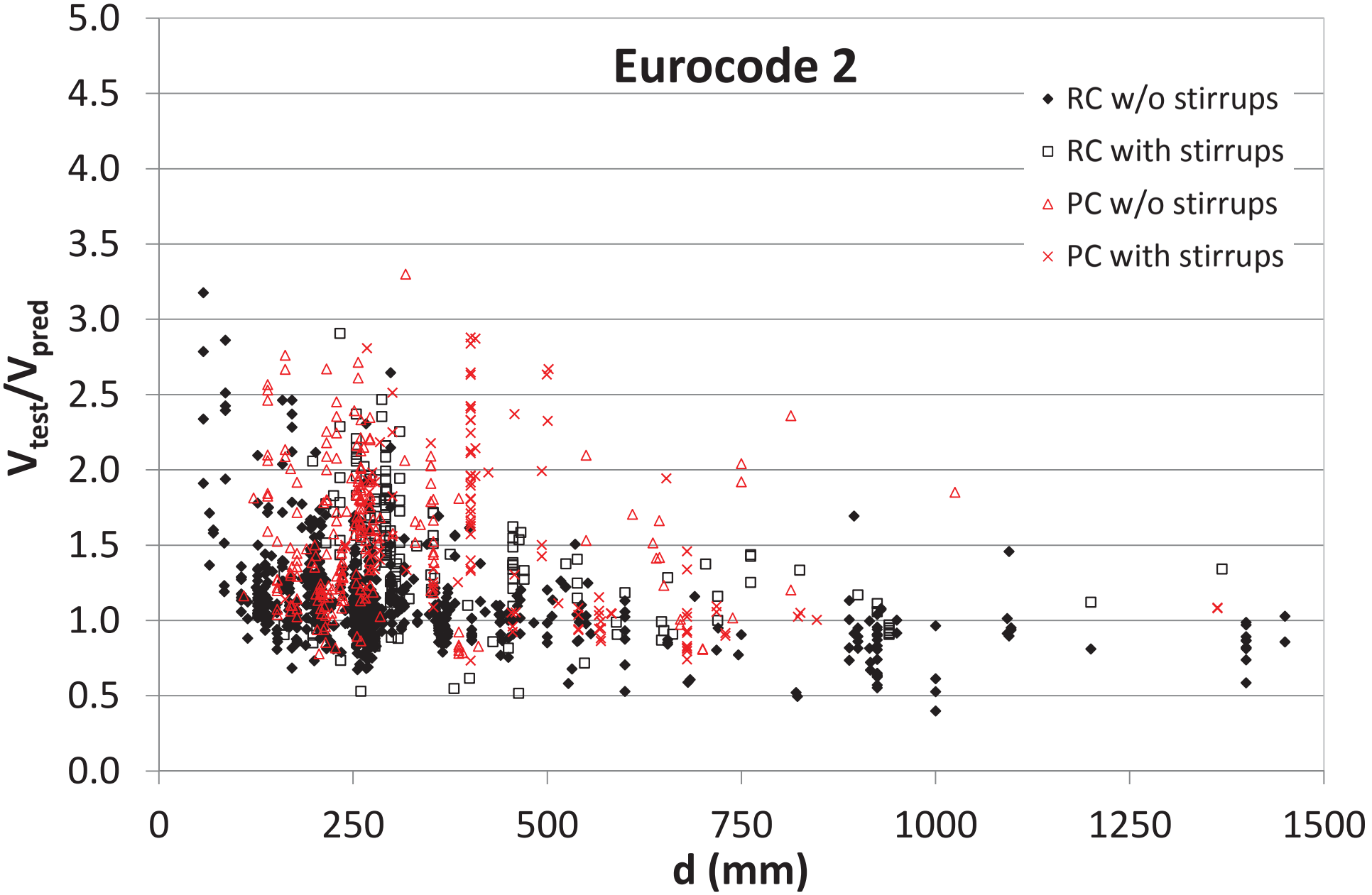

Figure 15c

Click here to download Figure Figure 15c.pdf

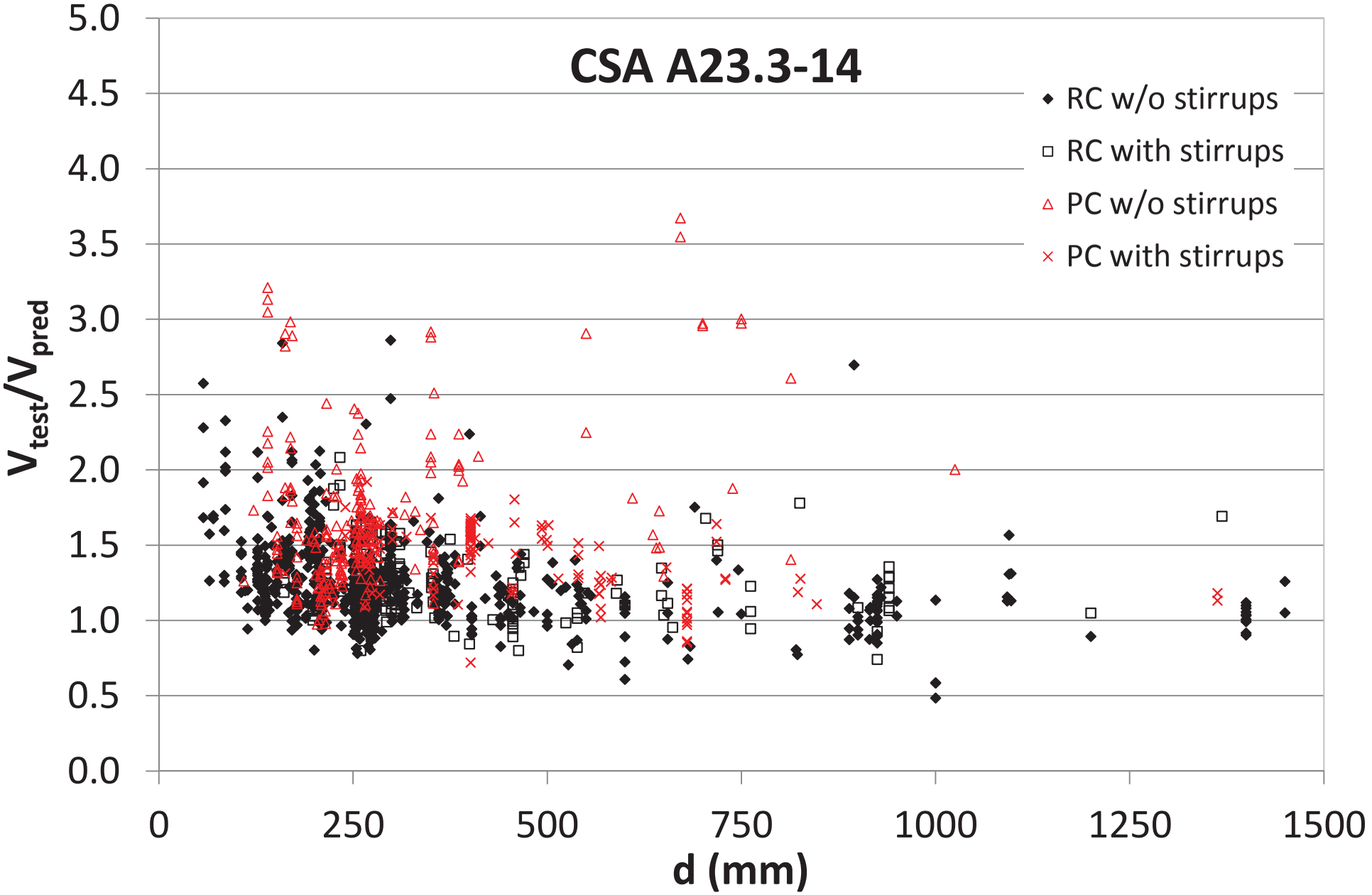

Figure 15d

Click here to download Figure Figure 15d.pdf

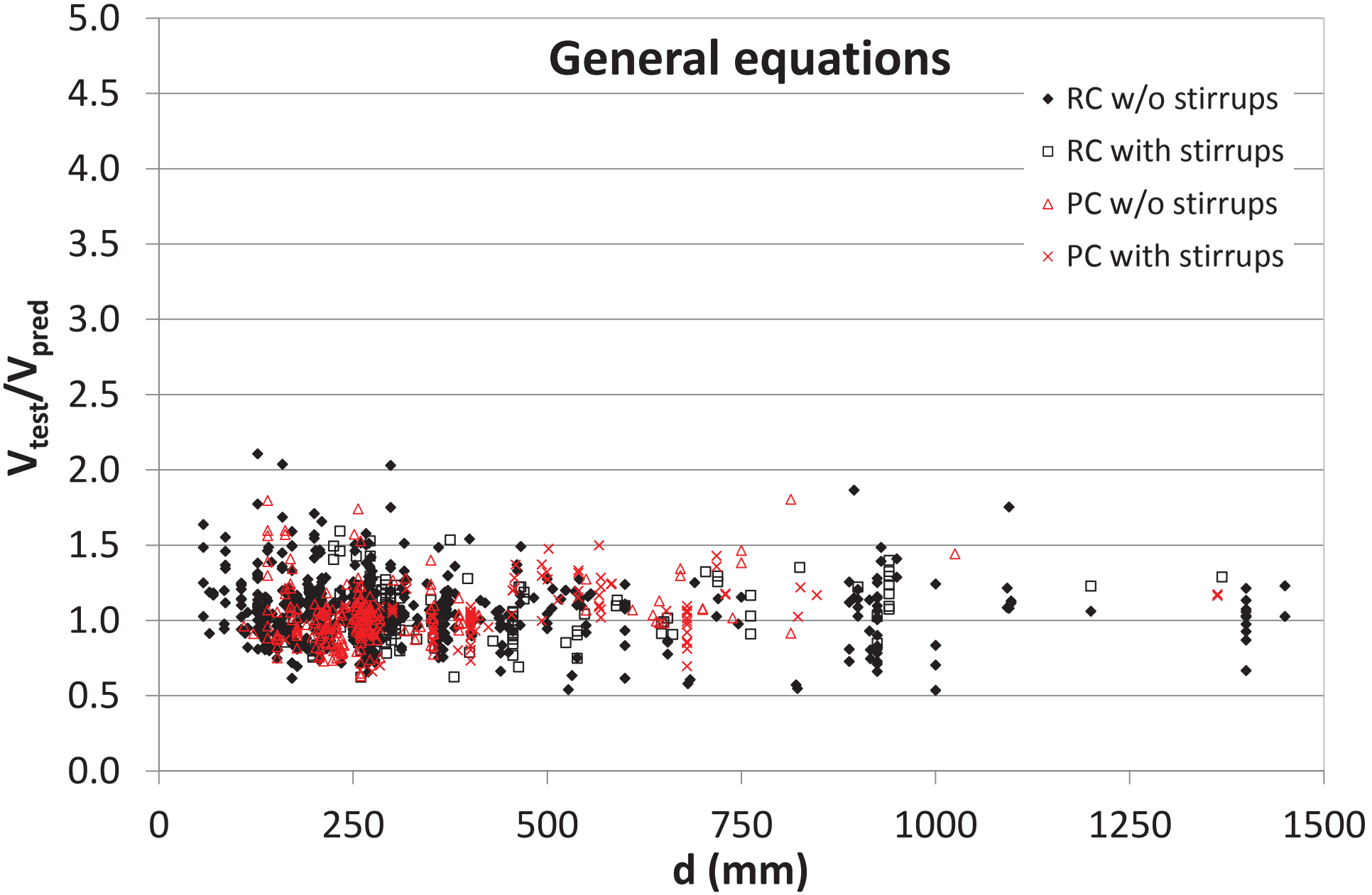

Figure 15e

Click here to download Figure Figure 15e.pdf

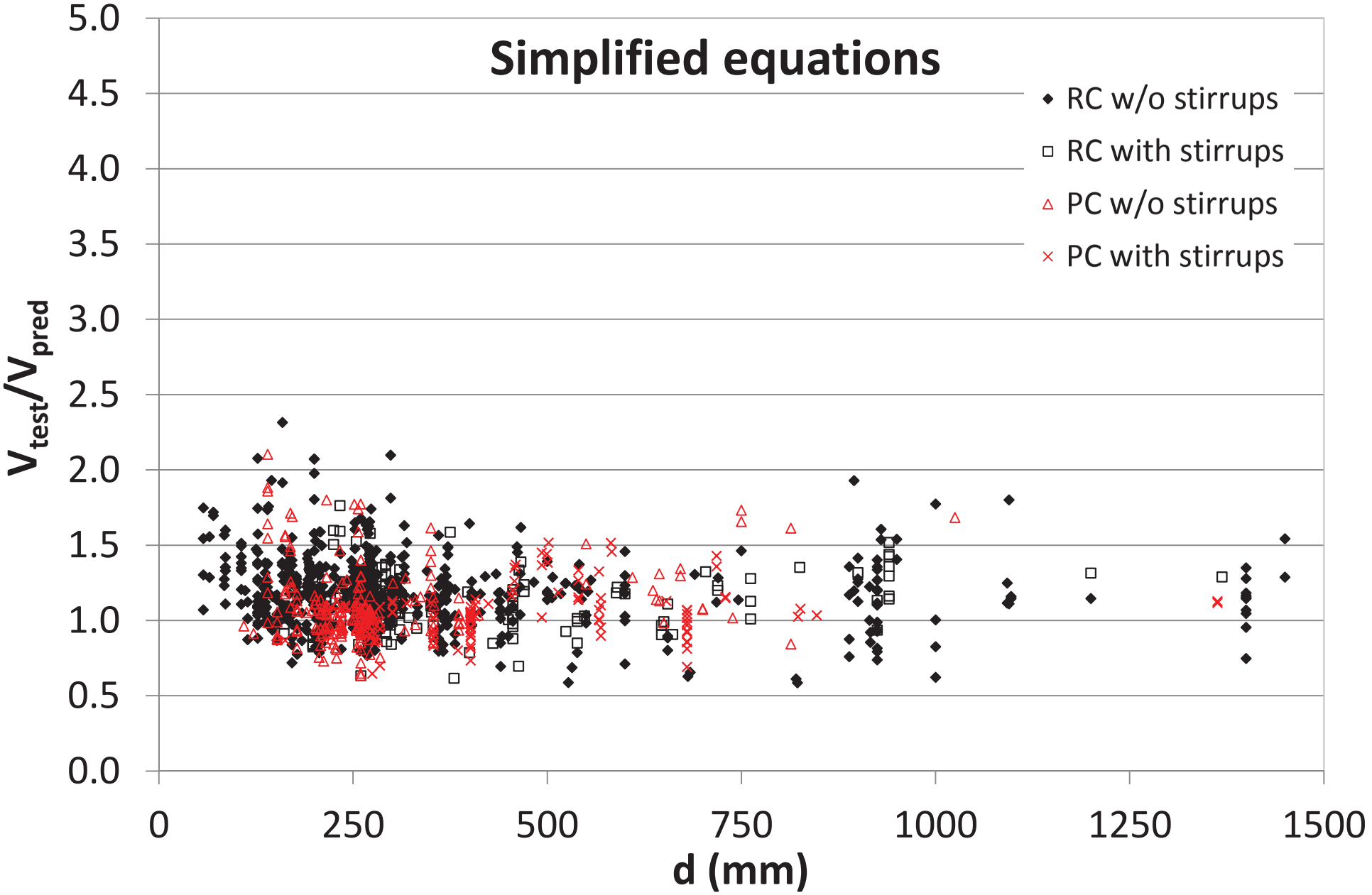

Figure 16a

Click here to download Figure Figure 16a.pdf

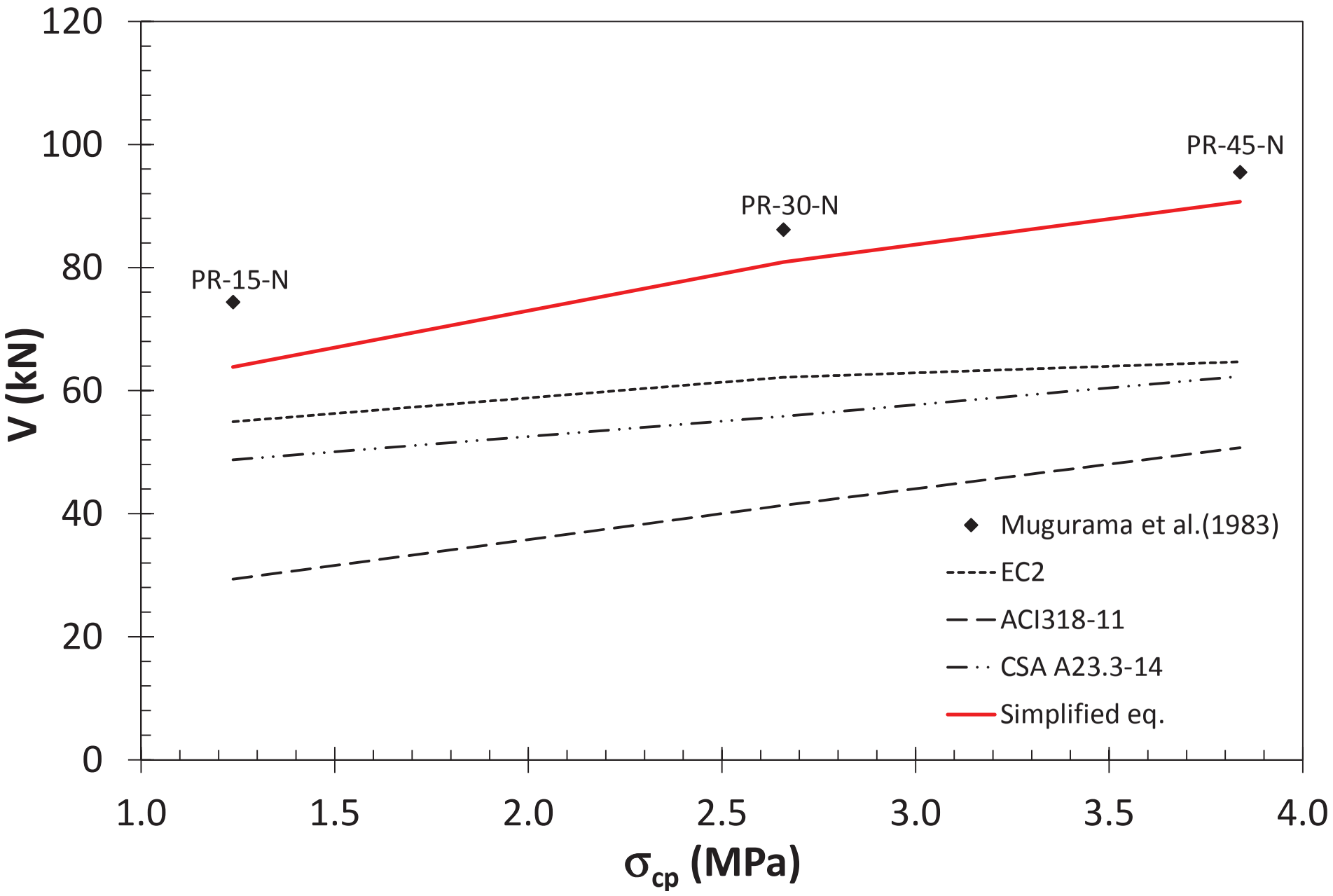

Figure 16b

Click here to download Figure Figure 16b.pdf

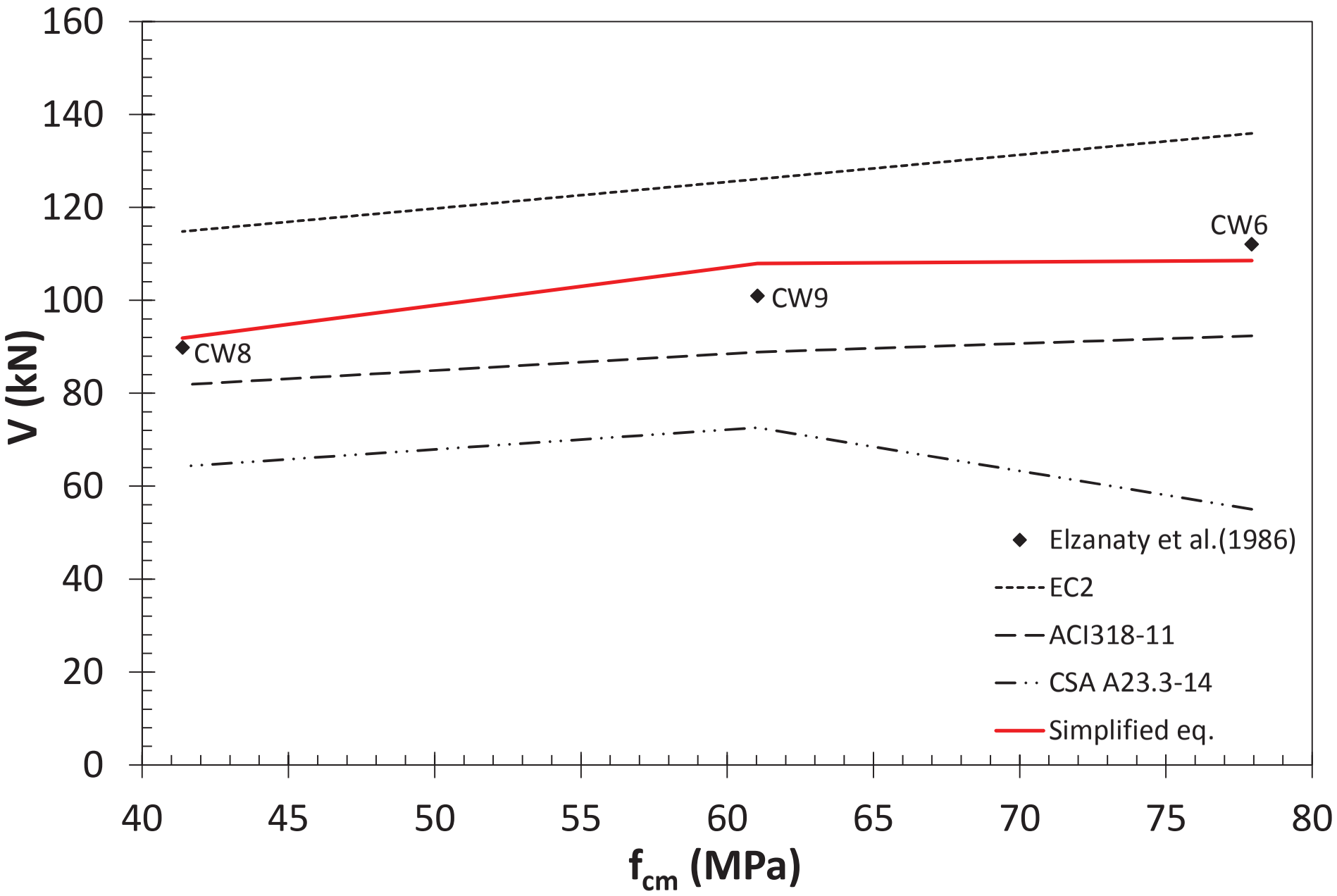

Figure 16c

Click here to download Figure Figure 16c.pdf

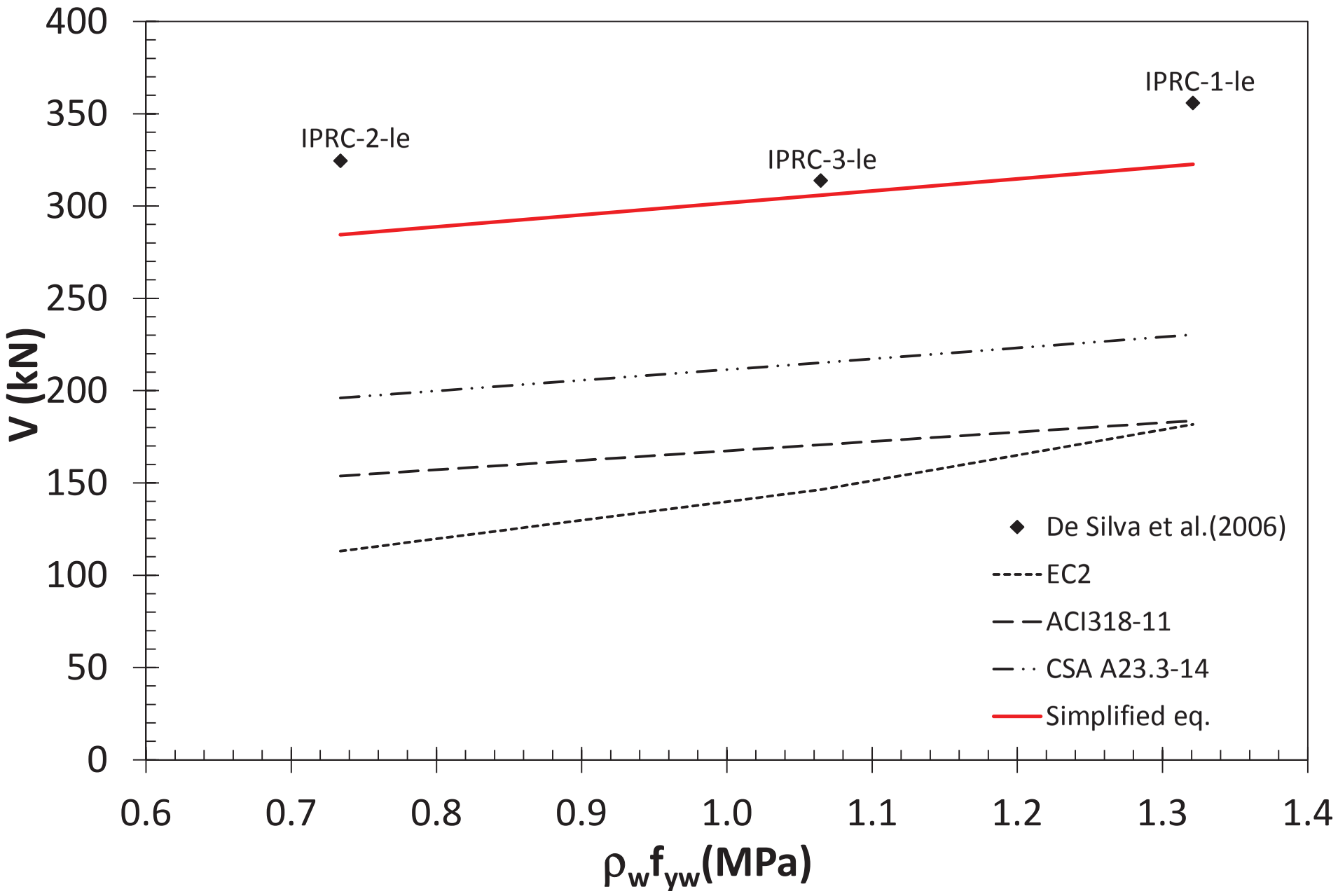

Figure 16d

Click here to download Figure Figure 16d.pdf

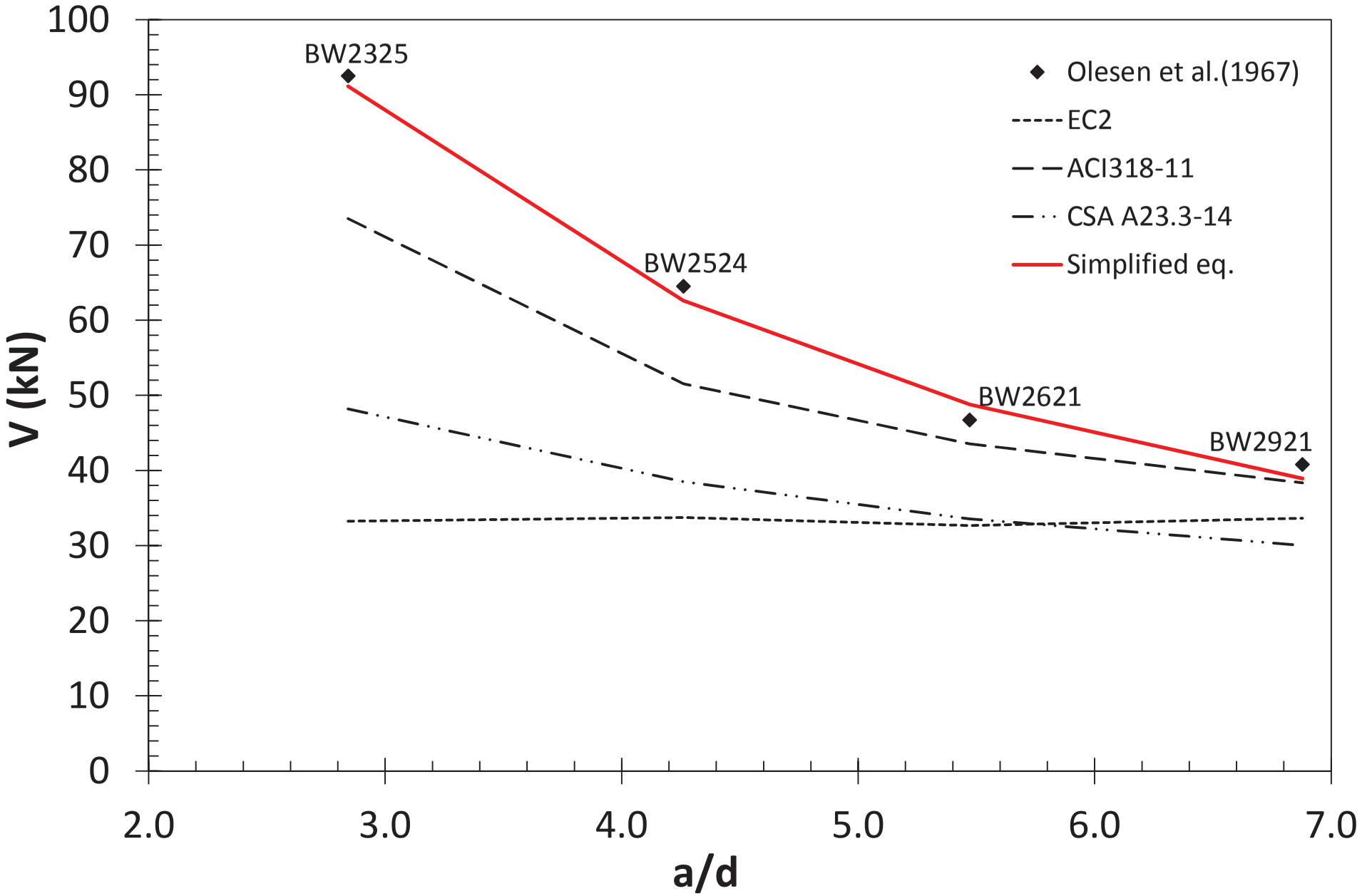

Figure 17

Click here to download Figure Figure 17.pdf

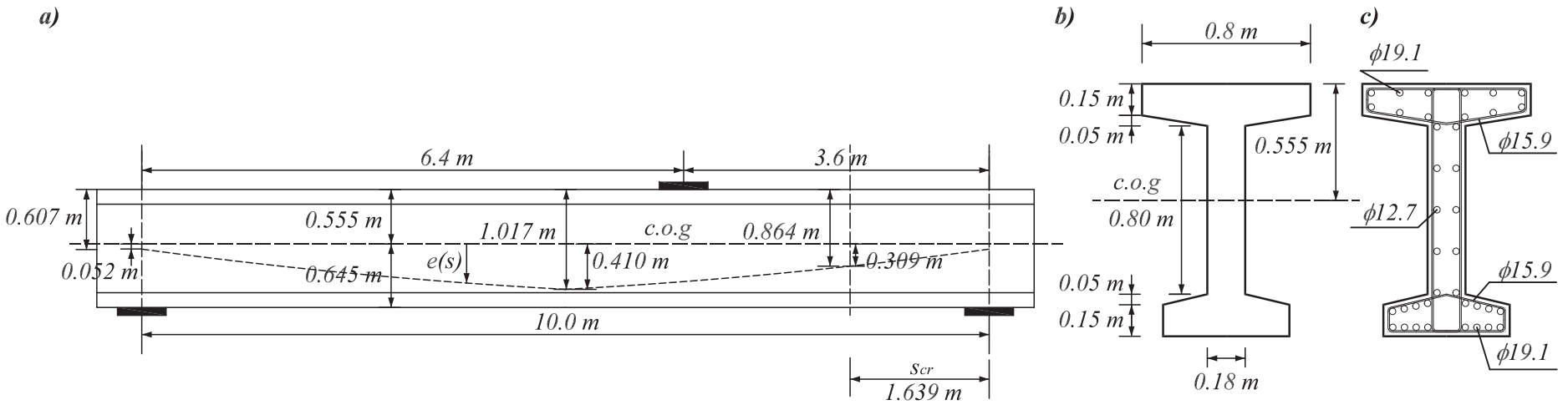

Fig. 1. Critical crack evolution under shear loading

Fig. 2. Numerical prediction of shear stresses under shear loading

Fig. 3. Adopted failure envelope for concrete under a biaxial stress state (Kupfer and Gerstle 1973)

Fig. 4. Shear-flexural crack patterns at failure in partially prestressed concrete beams (Maurer et al. 2014)

Fig. 5. Qualitative distribution of shear stresses at imminent shear failure and distribution

Fig. 6. Interpolation of neutral axis depth between reinforced and fully prestressed concrete

Fig. 7. Change of crack inclination when entering the flange

Fig. 8. Position of the shear critical section in the beam

Fig. 9. Position of the shear critical crack in reinforced and in prestressed concrete members

Fig. 10. Confinement stresses introduced by the stirrups in the un-cracked concrete zone

Fig. 11. Contribution of cracked concrete to shear resistance

Fig. 12. Forces acting on a rigid body part of a beam placed over the critical shear crack

Fig. 13. Normal and shear stresses and damage in a section of a prestressed beam

Fig. 14. Crack pattern at failure in a prestressed concrete girder without flexural cracks (Choulli et al. 2008; Choulli 2005)

Fig. 15. Correlation between the predictions and the experimental results as a function of the effective depth, *d*, for the 1285 beams included in the four ACI-DafStb databases

Fig. 16. Correlation between the predictions and experimental results for PC beams: a) influence of the amount of prestressing for rectangular beams w/o stirrups; b) influence of the concrete compression strength for beams w/o stirrups failing due to diagonal cracking; c) influence of the amount of stirrups in I-beams; d) Influence of the slenderness, *a/d*, for I-beams with stirrups

Fig. 17. Prestressed simply supported beam studied: prestressing layout and mid-span cross section